Monocyte chemoattractant protein (MCP)-1 deficiency ameliorates insulin resistance and fatty liver in lipoatrophic diabetic A-ZIP transgenic mice

脂肪萎縮性糖尿病 **A-ZIP Transgenic** マウスにおける

Monocyte chemo attractant protein (MCP)-1 の欠損は

インスリン抵抗性と脂肪肝を改善する

所属　：　糖尿病・代謝内科

指導教員　：　門脇　孝

申請者名　：　仁尾　泰徳

Contents

ABSTRACT

Monocyte chemo attractant protein (MCP)-1/chemokine (C-C motif) ligand (CCL) 2 (CCL2) secreted from white adipose tissue (WAT) in obesity has been reported to contribute to tissue macrophage accumulation and insulin resistance by inducing a chronic inflammatory state. MCP-1 has been shown to be elevated in the fatty liver of lipoatrophic A-ZIP- transgenic (A-ZIP-Tg) mice. Treatment of these mice with the CC chemokine receptor (CCR) 2 antagonist has been shown to ameliorate the hyperglycemia, hyperinsulinaemia and hepatomegaly, in conjunction with reducing liver inflammation. However, since CCR2 antagonists can block not only MCP-1 but also MCP-2 (CCL8) and MCP-3 (CCL7), it remains unclear whether MCP-1 secreted from the liver could contribute to hyperglycemia, hyperinsulinaemia and hepatomegaly in conjunction with liver inflammation, as well as to the M1 and M2 states of macrophage polarization. To address these issues, I analyzed the effects of targeted disruption of MCP-1 in A-ZIP-Tg mice. MCP-1 deficiency alone or per se resulted in a significant amelioration of insulin resistance in A-ZIP-Tg mice, which was associated with a suppression of extracellular signal-regulated protein kinase (ERK)-1/2 and p38 mitogen-activated protein kinase (p38MAPK) phosphorylation in liver. Although MCP-1 deficiency did not reduce the

expression of macrophage markers, it increased the expression of the genes encoding M2 macrophage markers such as *Arg1* and *Chi3l3*, as well as significantly reducing the triacylglycerol content of livers from A-ZIP-Tg mice. My data clearly indicated that MCP-1 deficiency improved insulin resistance and hepatic steatosis in A-ZIP-Tg mice and was associated with switching macrophage polarization and suppressing ERK-1/2 and p38MAPK phosphorylation.

INTRODUCTION

Obesity is a medical condition in which excess body fat has accumulated to the extent that it may have an adverse effect on health, leading to reduced life expectancy and/or increased health problems. Strong positive correlations exist between degree of adiposity and several obesity-associated disorder such as hypertension, atherosclerosis and glucose intolerance. Obesity increasing in much of the modern world (particularly in the Western world) and medical expenses for obesity leads to be a social problem. Expansion of adipose tissue is shown in obesity. Adipose tissue used to be thought to be a simple lipid accumulating tissue. Recently, it was revealed that adipose tissue was composed of not only adipocytes but also pre-adipocytes, macrophages, endothelial cells and fibroblasts, which are called stromal-vascular fraction (SVF). Adipocytes, also known as white fat cells, secrete many proteins called adipokines such as adiponectin, visfatin lipoprotein lipase and leptin. In addition, hypertrophic adipocytes caused by obesity secret inflammatory molecules such as TNF-α, IL-6 and monocyte chemo attractant protein -1 (MCP-1) (Fig. 1-1). Obesity is also associated with increased infiltration of macrophages into the adipose tissues. These adipose tissue macrophages (ATMs) are currently considered to be a major cause of obesity-associated chronic low-grade inflammation via the

secretion of a wide variety of inflammatory molecules [1, 2], including TNF-α, IL-6 [3] and MCP-1. These inflammatory molecules may have local effects on white adipose tissue (WAT) physiology as well as potential systemic effects on other organs that culminate in insulin resistance, metabolic syndrome and atherosclerosis. Although both hypertrophied adipocytes and infiltrated macrophages produce inflammatory cytokines, the extent of the amounts of secreted inflammatory cytokines from infiltrated macrophages which exist in SVF were higher than those from hypertrophied adipocytes [4]. Furthermore, Ito et al showed the process of secretion of inflammatory molecules and macrophage infiltration. They showed that MCP-1 mRNA expression was increased in hypertrophied adipocytes prior to macrophage accumulation in diet-induced obese mice. Thus, it was suggested that increase of MCP-1 mRNA expression in adipocyte was the trigger of macrophage infiltration in adipose tissue [5] (Fig. 1-2).

Among the inflammatory molecules up regulated in the adipose tissues of obese animals and humans, MCP-1 is a member of the cysteine–cysteine (C-C) chemokine family and promotes the migration of inflammatory cells by chemotaxis and integrin activation [6]. Both *Mcp-1* (also known as *Ccl2*) mRNA expression in WAT and plasma MCP-1 levels have been found to correlate positively with the degree of obesity in the individual [7]. In addition,

increased production of MCP-1 in WAT precedes the production of other macrophage markers during the development of obesity [8]. Mice overproducing MCP-1 in adipocytes showed macrophage recruitment in WAT and exhibited insulin resistance in the skeletal muscles (SKM) and liver (Fig. 1-3)[9]. Regarding the mechanisms, it was reported that MCP-1 stimulates the phosphorylation of extracellular signal-regulated protein kinase (ERK) through the C-C chemokine receptor (CCR) 2 [10] and activation of ERK-1/2 induces insulin resistance via decreased tyrosine phosphorylation of insulin receptor beta (IR-β) [9] as well as increased serine phosphorylation of IRS-1 [11].

Macrophage activation has been operationally defined across two separate polarization states: M1 and M2. M1, or 'classically activated', macrophages are induced by proinflammatory mediators such as lipopolysaccharide, whereas M2, or 'alternatively activated', macrophages generate high levels of anti-inflammatory cytokines such as IL-10, Arginase-1(Arg1), Chitinase 3-like 3 (Chi3l3) and TGF-β (Fig. 1-4)[12]. It was previously reported that disruption of MCP-1, or its receptor CCR2, in obese mice resulted in decreased macrophage infiltration in WAT and improved metabolic function [13, 14]. Moreover, ATMs from obese *Ccr2*-deficient mice produce M2 markers at levels similar to those seen in lean mice [14]. These data suggest that the MCP-1/CCR2 axis contributes to macrophage polarization.

Therefore, the phenotypic switch in ATM polarization is thought to lead to amelioration of insulin resistance.

In contrast to obesity, lipoatrophy is caused by a deficiency of WAT and is characterized by severe hepatic steatosis and insulin resistance. Lipoatrophy has been classified into four main categories: acquired partial lipoatrophy, acquired generalized lipoatrophy, familial partial lipoatrophy and congenital generated lipoatrophy. Lipoatrophy is also acquired after antiretroviral drug therapy. It is estimated that only a few thousand patients have this rare condition worldwide, although robust epidemiological data are not available. In addition, there have been no approved therapies for the treatment of metabolic abnormalities associated with lipoatrophy, with a combination of dietary modification, anti-diabetic medications and lipid-lowering agents used in the management of the condition. Due to lack of adipose tissue, there is almost no plasma leptin, one of the adipokines in lipoatrophy [15]. Recently, leptin-replacement clinical trial by using metreleptin, an analogue of human leptin, showed a sustained beneficial effect on diabetes and lipid control in lipoatrophy patients [16]. In near future, metreleptin therapy could be a first approval for lipoatrophy. As leptin also plays a regulatory role in immunity, inflammation, and hematopoiesis [17], it might lead to chronic inflammation in metreleptin treated lipoatrophy patients. Moreover, there is a concern about

emergence of neutralizing antibody for metreleptin. Thus, another treatment should be necessary.

Moitra and colleagues have generated lipoatrophic A-ZIP transgenic (A-ZIP-Tg) mice, which are profoundly insulin resistant and hyperlipidaemic [18–20]. These mice express a dominant-negative protein, termed A-ZIP, under the control of the adipose-specific aP2 enhancer/promoter. This protein prevents the DNA binding of B-ZIP transcription factors of both the C/EBP and Jun families. A-ZIP Tg mice have almost no white adipose tissue. They are initially growth delayed, but by week 12, surpass their littermates in weight. The mice eat, drink, and urinate copiously, have decreased fecundity, premature death, and frequently die after anesthesia. In addition, these mice exhibit severe hepatic steatosis and at the same time a chronic state of inflammation as indicated by high systemic levels of inflammatory cytokines such as IL-1β, IL-6, IL-12 and MCP-1 [21–23]. At the very least, MCP-1 is most abundantly expressed in the liver from A-ZIP-Tg mice [23]. Moreover, treatment of the lipoatrophic A-ZIP-Tg mice with a CCR2 antagonist has been shown to ameliorate the hyperglycaemia, hyperinsulinaemia and hepatomegaly, in conjunction with reducing liver inflammation. However, since CCR2 antagonist can block not only MCP-1, but also MCP-2 (chemokine [C-C motif] ligand [CCL] 8) and MCP-3 (also known as CCL7), it remains unclear whether MCP-1

secreted from liver could contribute to hyperglycaemia, hyperinsulinaemia and hepatomegaly in conjunction with liver inflammation, as well as to M1/M2 polarisation.

In this study, I hypothesised that MCP-1 secreted from the liver might also play an important role in the regulation of macrophage polarisation and insulin resistance-causing kinases such as ERK and p38 mitogen-activated protein kinase (p38MAPK) in liver. To address these issues, I analysed the effects of a targeted disruption of MCP-1 in lipoatrophic A-ZIP-Tg mice. I showed for the first time that a targeted disruption of MCP-1 alone in lipoatrophic diabetic A-ZIP-Tg mice resulted in decreased ERK-1/2 and p38MAPK phosphorylation and increased alternative M2 activation of macrophages, with at the same time an amelioration of insulin resistance and hepatic steatosis.
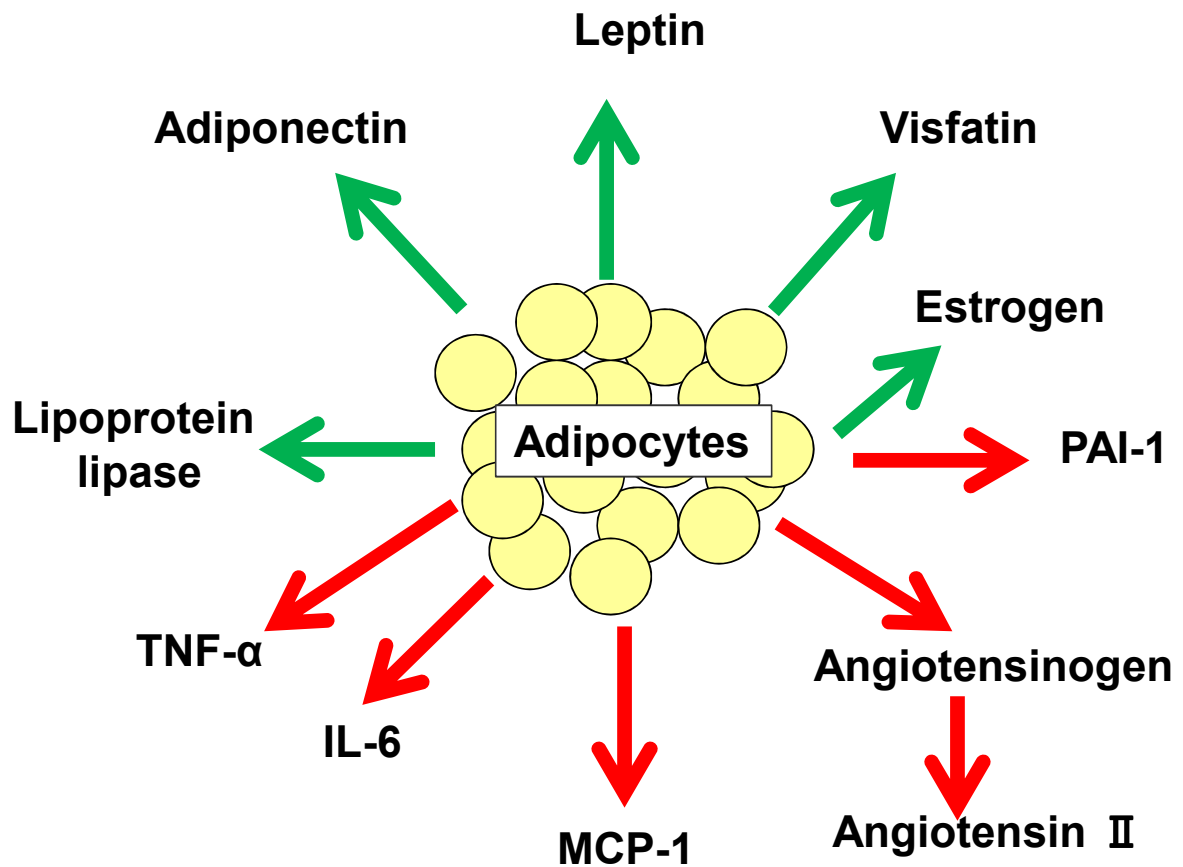
Fig. 1-1 Adipokines

Adipocytes secrete many proteins called adipokines such as adiponectin, visfatin lipoprotein lipase and leptin. In addition, hypertrophic adipocytes caused by obesity secret inflammatory molecules such as TNF-α, IL-6 and MCP-1.
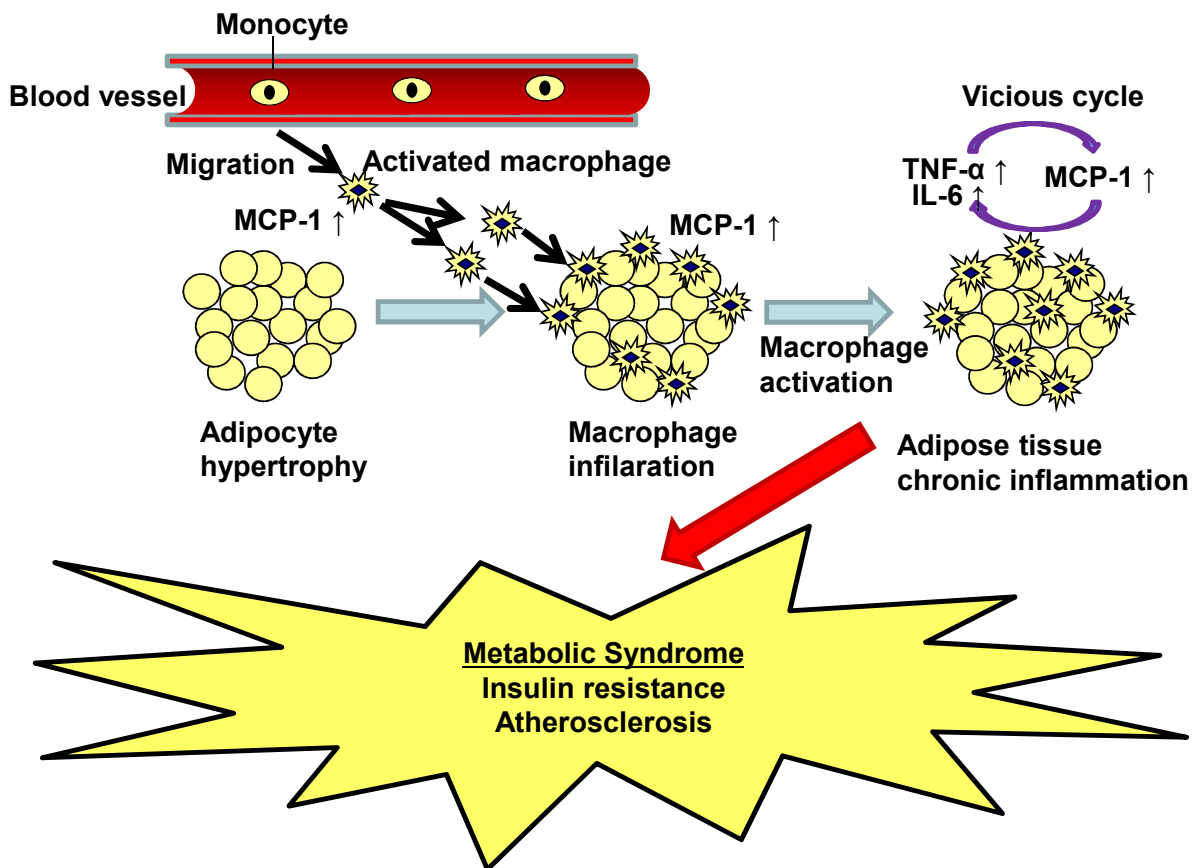
Fig. 1-2 Process of the acquirement of metabolic syndrome such as insulin resistance and atherosclerosis.

Hypertrophied adipocytes produce MCP-1 and induce migration of monocytes from blood vessels. Migrated monocytes are changed to activated macrophages by stimulation of MCP-1. These activated macrophages induce secretion of inflammatory molecules such as MCP-1 and TNF-α and it brings much activated macrophage infiltrations in adipose tissue. These negative inflammatory feedback called vicious cycle lead to become metabolic syndrome such as insulin resistance and atherosclerosis.
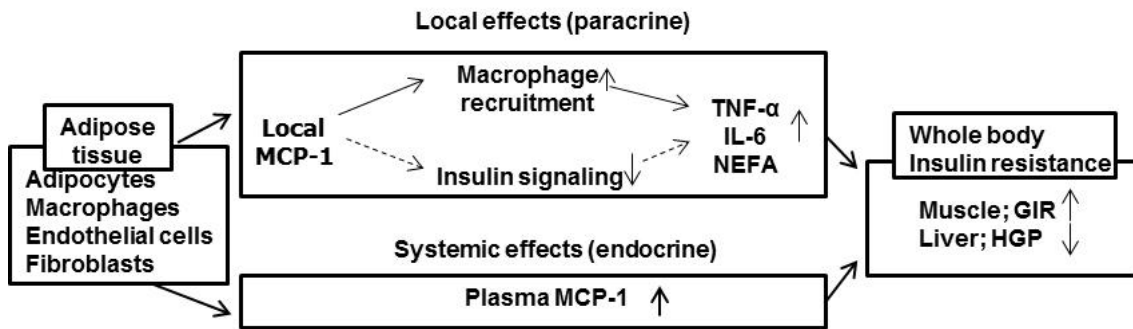
<u>Fig. 1-3 Overexpression of MCP-1 in adipose tissue results in systemic insulin resistance through both paracrine and endocrine pathways.</u>

Overexpression of MCP-1 in adipose tissue induced macrophage infiltration and at the same time increased insulin resistance causing adipokines, such as tumor necrosis factor-alpha (TNF-α), interleukin-6 (IL-6) and non-esteryzed free-fatty acids (NEFA), which resulted in systemic insulin resistance.
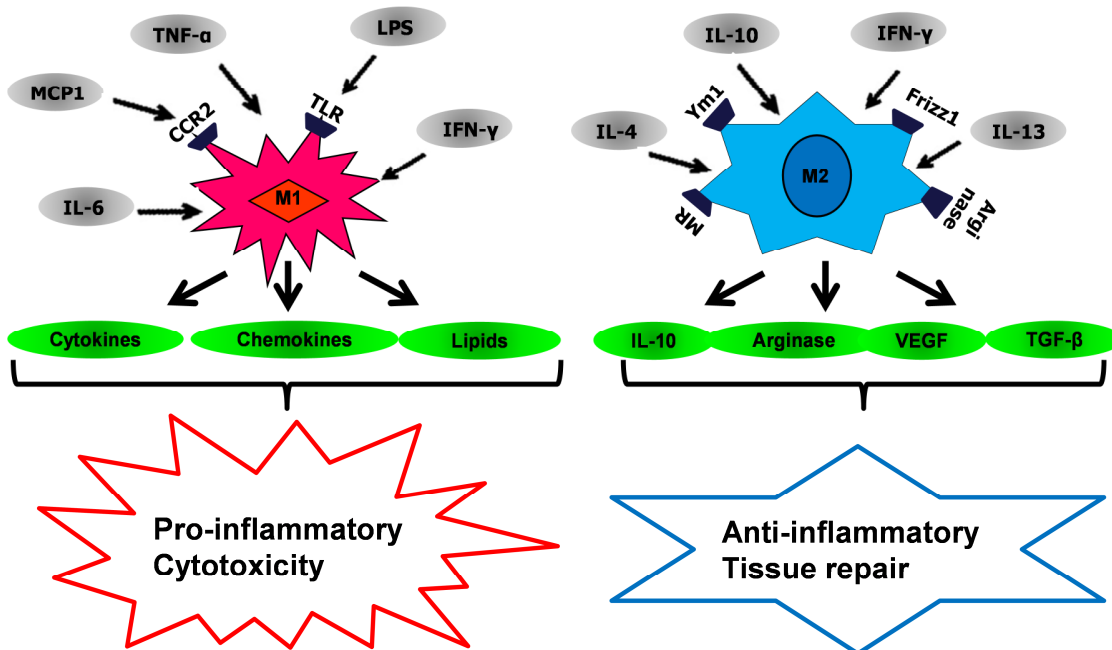

<u>Fig. 1-4 Macrophage polarization in response to inflammatory signals.</u>

Macrophage activation has been operationally defined across two separate polarisation states: M1 and M2. M1, or 'classically activated', macrophages are induced by pro-inflammatory mediators such as lipopolysaccharide, whereas M2, or 'alternatively activated', macrophages generate high levels of anti-inflammatory cytokines such as IL-10, Arginase and TGF-β.

PURPOSE OF THIS STUDY

To address the effects and mechanisms of MCP-1 derived from tissues other than WAT, such as

fatty liver for the regulation of whole body insulin sensitivity, hepatic steatosis and macrophage

polarization by using lipoatrophic A-ZIP transgenic mice.

MATERIALS AND METHODS

Generation of A-ZIP-Tg×Mcp1$^{-/-}$ mice

A-ZIP/F-1 (A-ZIP-Tg) mice were generous gifts from C. Vinson of the National Cancer Institute at Frederick, MD, USA. $Mcp1^{-/-}$ mice were purchased from the Jackson Laboratory (Bar Harbor, ME, USA) and C57BL/6 mice from CLEA Japan (Fujinomiya, Shizuoka, Japan). A-ZIP/F-1 mice were on an FVB/N (FVB) background. MCP-1 homozygous-knockout mice were on a C57BL/6 background, which had been backcrossed to C57BL/6 mice for 10 generations.

To generate A-ZIP-Tg $Mcp1^{+/-}$ mice, conceptuses that were obtained by in vitro fertilisation of ova from $Mcp1^{-/-}$ mice and sperm from A-ZIP-Tg mice were implanted into pseudo-pregnant foster mothers as previously described [24]. To generate A-ZIP-Tg×MCP-1 knockout ($Mcp1^{-/-}$) mice and $Mcp1^{-/-}$ mice, conceptuses that had been obtained by in vitro fertilisation of ova from MCP-1 homozygous-knockout mice and sperm from A-ZIP-Tg×MCP-1 heterozygous-knockout mice were implanted into pseudo-pregnant foster mothers. To generate wild-type (WT) mice and A-ZIP-Tg mice, conceptuses that had been obtained by in vitro fertilisation of ova from C57BL/6 mice and sperm from A-ZIP-Tg×MCP-1

heterozygous-knockout mice were implanted into pseudo-pregnant foster mothers. All experiments in this study were conducted on female mice.

In this study, I generated WT mice, $Mcp1^{-/-}$ mice, A-ZIP-Tg mice and A-ZIP-Tg×$Mcp1^{-/-}$ mice which were on an FVB/B6 F2 background. This breeding strategy was used to improve the viability of the offspring as A-ZIP-Tg mice on an FVB background have poor survival [18].

Mice

Mice were housed in cages and maintained on a 12-h light/dark cycle. For all experiments, the diet was standard chow (CE-2; CLEA Japan) with the following composition: 25.6% (wt/wt) protein, 3.8% fibre, 6.9% ash, 50.5% carbohydrates, 4% fat and 9.2% water [24–26]. The animal care and use procedures were approved by the Animal Care Committee of the University of Tokyo.

Northern blot analysis

Northern blotting was carried out according to the method described previously [25, 26]. Total RNA was extracted from various tissues with TRIzol reagent according to the

14

manufacturer's instructions (Invitrogen, Carlsbad, CA, USA). Total RNA (15 μg) was loaded

onto a 1.3% agarose gel and transferred to a nylon membrane (Hybond N+; GE Healthcare Life

Sciences, Hino, Tokyo, Japan). MCP-1 coding sequence cDNA was used as the probe template.

The cDNA probe template of MCP-1 was prepared by RT-PCR using specific primers. The

forward primer was 5'-CCATGCAGGTCCCTGTC-3' and the reverse primer was

5'-CTAGTTCACTGTCACAC-3', as previously described [9]. The corresponding bands were

quantified by exposure of BAS2000 to the filters and measurement with BAStation software

(Fuji Film, Minato-ku, Tokyo, Japan).

Real-time quantitative PCR

For real-time quantitative PCR analysis, cDNA synthesised from total RNA was

analysed. For quantification of gene expression, a set of predesigned primers and probes for

each gene (Assays-on-Demand; Applied Biosystems, Carlsbad, CA, USA) were used.   Mouse

MCP-1: Mm00441242_m1,

mouse MCP-2: Mm01297183_m1,

mouse MCP-3: Mm00443113_m1,

mouse CCR2: Mm99999051_gH,

mouse Emr1: Mm00802530_m1,

mouse CD68: Mm00839636_g1,

mouse Chi3l3: Mm00657889_mH,

mouse TGF-β: Mm03024053_m1,

mouse Arg1: Mm01190441_g1,

mouse PPARa: Mm00440949_m1,

mouse Acyl-coA oxidase: Mm00443579_m1,

mouse UCP2: Mm00495907_g1,

mouse SREBP1c: Mm00550338_m1,

mouse SCD1: Mm00772290_m1.

The primer sets and the probe for mouse cyclophilin were as follows:

the forward primer was 5'-GGTCCTGGCATCTTGTCCAT-3',

the reverse primer was 5'-CAGTCTTGGCAGTGCAGATAAAA-3';

and the probe was 5'-CTGGACCAAACACAAACGGTTCCCA-3'.

The relative amount of each transcript was normalised to the amount of mouse cyclophilin

mRNA.

Blood sample assays and in vivo glucose homeostasis

Glucose tolerance tests (GTTs) were conducted as previously described with slight modifications [25, 26]. For the GTTs, mice were deprived of food for 6 h and then orally administered with D-glucose (1.5 g per kg body weight). Plasma glucose and plasma triglycerol (TG) levels in the fed state were determined using a glucose B-test and TG E-type test (Wako Pure Chemical Industries, Yodogawa-ku, Osaka, Japan), respectively. Plasma insulin levels were measured with an insulin immunoassay (Shibayagi, Shibukawa, Gunma, Japan). Plasma MCP-1 levels in the fed state were measured using a mouse immunoassay kit (Pierce Biotechnology Inc, Rockford, IL, USA).

Hyperinsulinemic-euglycemic clamp study

Clamp studies were carried out between A-ZIP-Tg mice and A-ZIP-Tg×*Mcp1*^{-/-} mice. Data represent means±SEM (n=3 per group).*$P<0.05$ vs A-ZIP-Tg mice. 2-3 days before the study, an infusion catheter was inserted into the right jugular vein under general anesthesia with sodium pentobarbital. Studies were performed on mice under conscious and unstressed conditions after a 6-h fast. A primed continuous infusion of insulin (Humalin R, Lilly) was given (5.0 mill units/g/min), and the blood glucose concentration, monitored every 5 min, was

maintained at (11 m moll/l) by administration of glucose (5g of glucose per 10 mL enriched to 20% with [6,6-2H2] glucose (Sigma)) for 120 min. Blood was sampled via tail tip bleeds at 90, 105, and 120 min for determination of exogenous glucose infusion rates (GIR), hepatic glucose production (HGP) and rate of glucose disappearance (Rd).

Antibodies

Mouse monoclonal anti-phosphotyrosine antibody 4G10 (αPY) was purchased from Merck Millipore (Billerica, MA, USA). Rabbit polyclonal antibody to IR-β was purchased from Santa Cruz Biotechnology (Santa Cruz, CA, USA). Rabbit polyclonal antibodies against ERK-1/2, phospho-ERK-1/2 (Thr202/Tyr204), p38MAPK, phosphor-p38MAPK (Thr180/Tyr182), insulin, hemoxygenase-1, Akt and phospho-Akt (Ser-473) were purchased from Cell Signaling Technology (Danvers, MA, USA). Rabbit polyclonal antibodies against IRS-1 and phospho-IRS-1 (Ser-612) were purchased from Cell Signaling Technology (Danvers, MA, USA).

Immunoblotting and immunoprecipitation

Immunoblotting and immunoprecipitation were conducted as previously described [27]. In brief, in the fed state, the skeletal muscles from the hind limbs or livers were removed. The samples were homogenised in ice-cold 1% Nonidet P-40-buffer (25 mmol/l Tris-HCL [pH 7.4], 10 mmol/l sodium orthovanadate, 10 mmol/l EGTA and 1 mmol/l phenylmethylsulfonyl fluoride) and centrifuged. For immunoblotting, muscle homogenates containing 5 mg of total protein or liver homogenates containing 15 mg of total protein were incubated with the indicated primary antibodies and horseradish peroxidase-conjugated anti-mouse-IgG secondary antibody and were detected with enhanced chemiluminescence (ECL) reagent (GE Healthcare Life Sciences). For immunoprecipitation, muscle homogenates containing 5 mg of total protein or liver homogenates containing 15 mg of total protein were also incubated with the indicated antibodies followed by addition of protein G-Sepharose. The immunoprecipitates were washed with 1% Nonidet P-40-buffer 3 times. The immunoprecipitates were subjected to immunoblotting with the indicated primary antibodies and horseradish peroxidase-conjugated anti-mouse-IgG secondary antibody and were detected with ECL reagent.

Histological analyses and TG content in liver

Livers from WT mice, A-ZIP-Tg mice and A-ZIP-Tg×*Mcp1*$^{-/-}$ mice were fixed

overnight in 10% formalin (vol./vol.). Samples were routinely embedded in paraffin.

Approximately 5 μm-thick slices obtained from these liver samples were stained with

haematoxylin and eosin. The liver homogenates were extracted and their TG content was

determined as previously described [24].

Macrophage staining in liver

Livers from WT mice, A-ZIP-Tg mice and A-ZIP-Tg×*Mcp1*$^{-/-}$ mice were fixed

overnight in 10% formalin (vol./vol.). Samples were routinely embedded in paraffin.

Approximately 5 μm-thick slices obtained from these liver samples were stained with

anti-hem-oxygenase-1 (HO-1) as previously described [28].

Insulin staining in islet

Islets from WT mice, A-ZIP-Tg mice and A-ZIP-Tg×*Mcp1*$^{-/-}$ mice were fixed

overnight in 10% formalin (vol./vol.). Samples were routinely embedded in paraffin.

Approximately 5 μm-thick slices obtained from these islet samples were stained by using anti-insulin antibody as previously described [29].

Cuff injury model

The cuff injury model was used as described previously [30]. The left femoral artery was isolated from surrounding tissues, and after loosely sheathing it with a 2.0-mm polyethylene cuff mode of PD-50 tubing, the cuff was tied in place with an 80 suture. The cuffs were larger than the vessels and did not obstruct blood flow. 2 weeks after cuff placement, vessels were foxed with 10% formalin and embedded in paraffin. Continuous cross-sections were cut from one end of the cuffed portion to the other end and were stained for elastic fibers and with hematoxylin and eosin. The thickness of the neo intimal formation was observed by digital microscope camera (Olympus, Tokyo, japan).

Statistical analysis

Results are expressed as means±SEM. The Student's *t* test was performed to compare two groups. Values p<0.05 were considered statistically significant.

RESULTS

No differences in body weight, plasma glucose levels and liver weight between WT mice and *Mcp1*$^{-/-}$ mice.

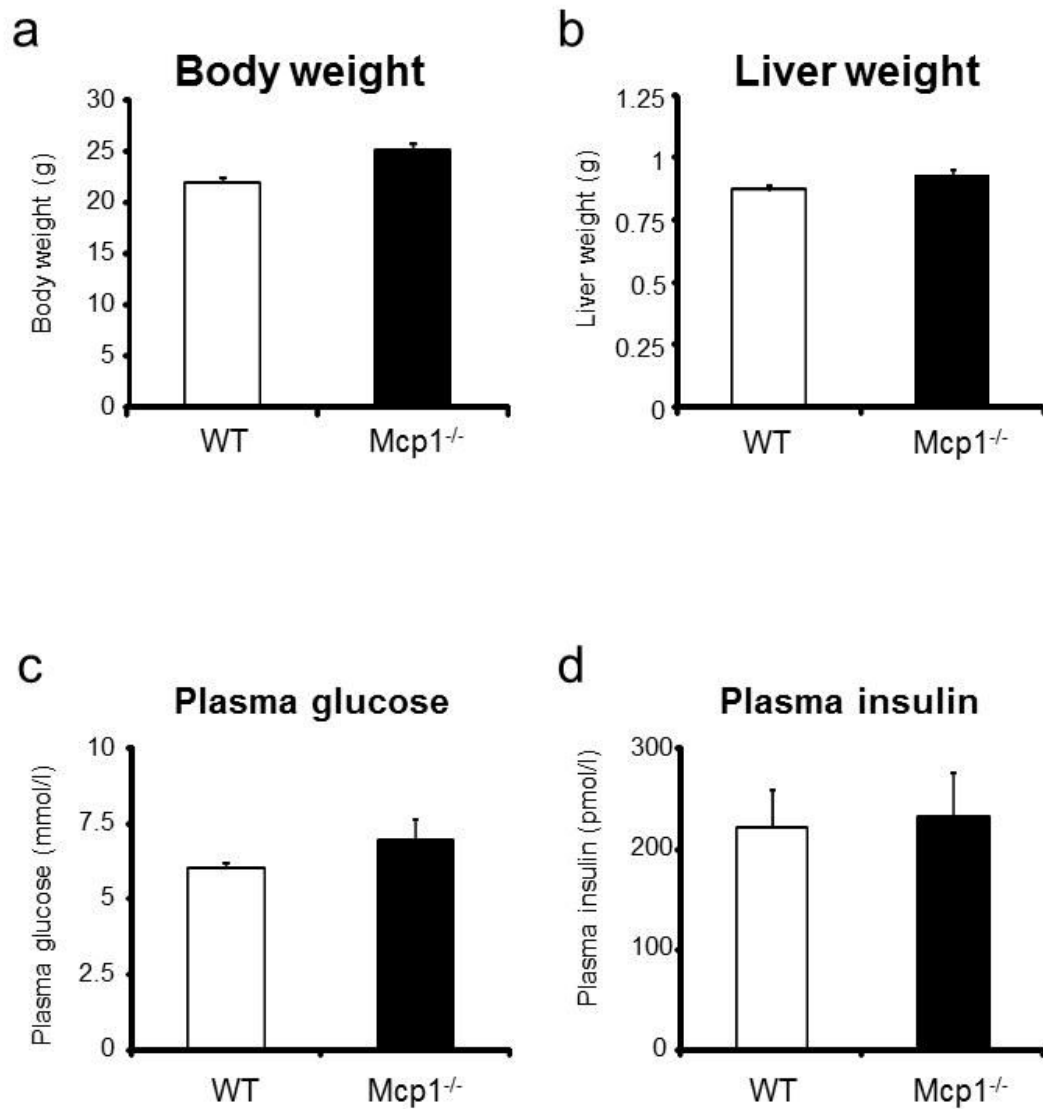As there was no difference in body weight, plasma glucose levels in the fed state and liver weight between WT mice and *Mcp1*$^{-/-}$ mice (Fig. 2), and previous reports had also shown that the body weight, adipose weight, insulin tolerance and glucose tolerance of *Mcp1*$^{-/-}$ mice fed normal chow did not differ from those of WT control mice [13], I analyzed and compared the WT mice, A-ZIP-Tg mice and A-ZIP-Tg×*Mcp1*$^{-/-}$ mice.

Fig. 2 There was no difference in body weight, plasma glucose levels in the fed state and liver weight between WT mice and *Mcp1*$^{-/-}$ mice

Body weight of WT mice and *Mcp1*$^{-/-}$ mice were measured at 9 weeks of age, as indicated (a). Liver weight of WT and *Mcp1*$^{-/-}$ 15-week-old mice (b). Plasma parameters of glucose (c) and insulin (d) were measured in 15-week-old WT and *Mcp1*$^{-/-}$ mice. Data represent means±SEM (WT mice, *n*=5, *Mcp1*$^{-/-}$ mice, *n*=5). **P<0.01 vs WT mice.

Gender difference in MCP-1 deficient A-ZIP-Tg mice.

In the beginning of this study, I compared the gender phenotypic difference of MCP-1 deficient A-ZIP-Tg mice. The increase in plasma MCP-1 level of A-ZIP-Tg male mice (Fig. 3a) was similar to that of A-ZIP-Tg female mice (Fig. 3a). MCP-1 deficiency significantly ameliorated hyperglycaemia (Fig. 3b) but not hyperinsulinaemia in A-ZIP-Tg male mice (Fig. 3c). Plasma glucose levels and plasma insulin levels during the GTTs were not significantly changed in male A-ZIP-Tg×$Mcp1^{-/-}$ mice as compared with male A-ZIP-Tg mice (Fig. 3d,e), suggesting that MCP-1 deficiency in male A-ZIP-Tg mice did not ameliorate glucose intolerance. These data suggested that the insulin-sensitive phenotype of A-ZIP-Tg- $Mcp1^{-/-}$ mice was prominent in female mice compared with male mice. I thus used female mice in this study.
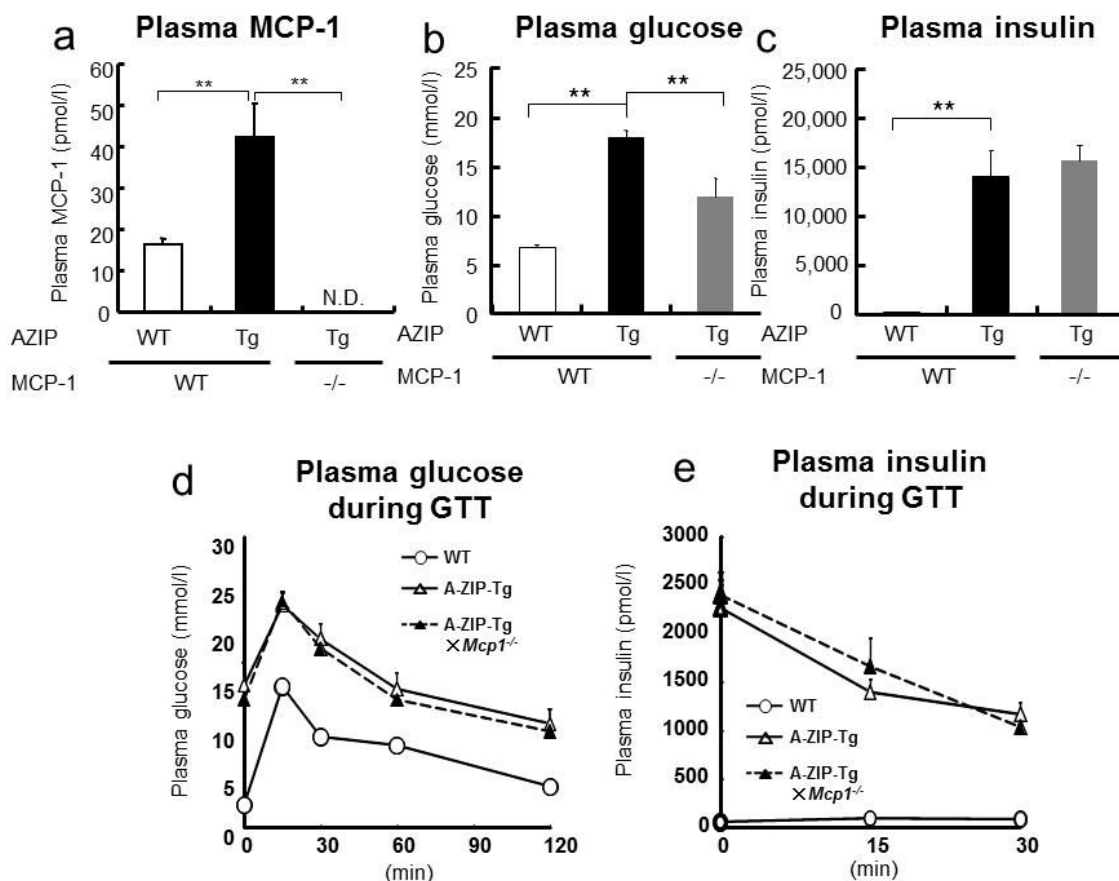
24

Fig. 3 MCP-1 deficiency in male A-ZIP-Tg mice ameliorates hyperglycemia but not hyperinsulinaemia.

Plasma parameters of MCP-1 (a), glucose (b) and insulin (c) were measured in 15-week-old WT (white bars), A-ZIP-Tg (black bars), and A-ZIP transgenic MCP-1 knockout (A-ZIP-Tg×$Mcp1^{-/-}$) (grey bars) mice. Plasma glucose (d) and plasma insulin (e) during GTT (1.5 g glucose per kilogram body weight) in WT (white circles), A-ZIP-Tg (white triangles) and A-ZIP-Tg×$Mcp1^{-/-}$ (black triangles) in 15-week-old mice. Data represent means ± S.E.M. (WT mice, $n = 5$; A-ZIP-Tg mice, $n = 16$; and A-ZIP-Tg×$Mcp1^{-/-}$ mice, $n = 11$). * $P < 0.05$ versus A-ZIP-Tg×$Mcp1^{-/-}$ mice.

25

Plasma MCP-1 concentration and Mcp-1 mRNA expression in fatty liver were increased in lipoatrophic A-ZIP-Tg mice

Many previous studies have reported elevated plasma MCP-1 concentration and *Mcp-1* mRNA expression in WAT of obese and diabetic mice [9, 13, 31–33]. As reported [23], plasma MCP-1 concentrations were significantly elevated in A-ZIP-Tg mice compared with WT mice (Fig. 4a). A previous study showed that, in WT mice, *Mcp-1* mRNA was not detected in any tissues [13], whereas in A-ZIP-Tg mice, as previously reported [23], *Mcp-1* mRNA was most abundantly expressed in the liver among all the tissues I examined, including brown adipose tissue (BAT), except for WAT, because lipoatrophic A-ZIP-Tg mice still have BAT but not WAT, as reported in other studies [14, 18, 19, 23] (Fig. 4b). It has been reported that MCP-1 is abundantly expressed in Kupffer cells, as well as in hepatocytes in the liver [34, 35]

a

Plasma MCP-1

A-ZIP   WT   Tg   Tg

MCP-1   WT   -/-

b

A-ZIP-Tg

Liver   SKM   BAT   Hypo   Ovary
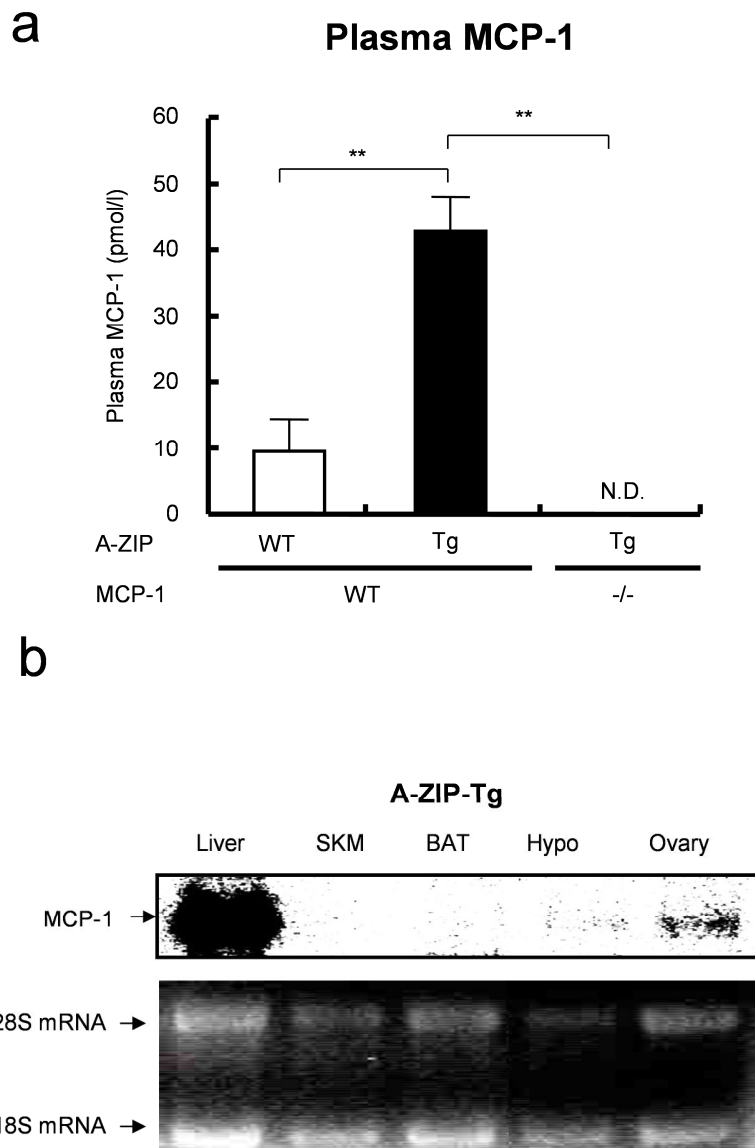
MCP-1 →

28S mRNA →

18S mRNA →

Fig. 4 Plasma MCP-1 concentration and tissue distribution of *Mcp1* mRNA in A-ZIP-Tg mice.
(a) Plasma concentrations of MCP-1 were measured in WT (white bars), A-ZIP-Tg (black bars) and A-ZIP-Tg×*Mcp1*$^{-/-}$ (grey bars) 15-week-old mice in the fed state. Data are means±SEM. WT mice, *n*=5; A-ZIP-Tg mice, *n*=17; A-ZIP-Tg×*Mcp1*$^{-/-}$ mice, *n*=16. **p<0.01 vs A-ZIP-Tg mice. ND, not detected. (b) Northern blot analysis of *Mcp1* mRNA expressed in liver, SKM, BAT, Hypo (hypothalamus) and ovary of 15-week-old A-ZIP-Tg mice

MCP-1 deficiency decreased body weight gain and liver weight in A-ZIP-Tg mice

To clarify the pathophysiological roles of elevated MCP-1 levels in lipoatrophic A-ZIP-Tg mice, I generated A-ZIP-Tg×$Mcp1^{-/-}$ mice. MCP-1 deficiency in A-ZIP-Tg mice resulted in decreased body weight compared with A-ZIP-Tg mice (Fig. 5a), although the food intake of A-ZIP-Tg×$Mcp1^{-/-}$ mice was not significantly different from that seen in A-ZIP-Tg mice (Table 1). Furthermore, the liver weight of A-ZIP-Tg×$Mcp1^{-/-}$ mice was decreased compared with that of A-ZIP-Tg mice (Fig. 5b).

Table 1.

Food intake of A-ZIP-Tg mice and A-ZIP-Tg×$Mcp1^{-/-}$ mice.

	A-ZIP-Tg	A-ZIP-Tg×$Mcp1^{-/-}$ mice
Food intake (g/day)	5.93±0.18	4.31±0.09*
Food intake (g/day/BW)	0.20±0.01	0.17±0.02
Body weight (g)	29.67±1.35	25.33±0.98**

Average food intake per day, average food intake per day per body weight and average body weight of A-ZIP-Tg and A-ZIP-Tg×$Mcp1^{-/-}$ were measured from 11-14 weeks of age. Data represent means±SEM (A-ZIP-Tg mice, n=17 and A-ZIP-Tg×$Mcp1^{-/-}$ mice, n=16). *$P<0.05$, **$P<0.01$ vs A-ZIP-Tg mice.

Table 2.

Tissue weight of A-ZIP-Tg mice and A-ZIP-Tg×$Mcp1^{-/-}$ mice.

	A-ZIP-Tg	A-ZIP-Tg×$Mcp1^{-/-}$ mice
Body weight (g)	31.53±0.76	26.91±0.80**
Liver weight (g)	3.12±0.27	2.22±0.29**
BAT weight (g)	0.03±0.01	0.02±0.01
Pancreas weight (g)	0.45±0.02	0.42±0.04

Body weight, liver weight, BAT weight and Pancreas weight of   A-ZIP-Tg and A-ZIP-Tg×$Mcp1^{-/-}$ were measured at 15-week-old mice. Data represent means±SEM (A-ZIP-Tg mice, n=17 and A-ZIP-Tg×$Mcp1^{-/-}$ mice, n=16). *$P<0.05$, **$P<0.01$ vs A-ZIP-Tg mice.
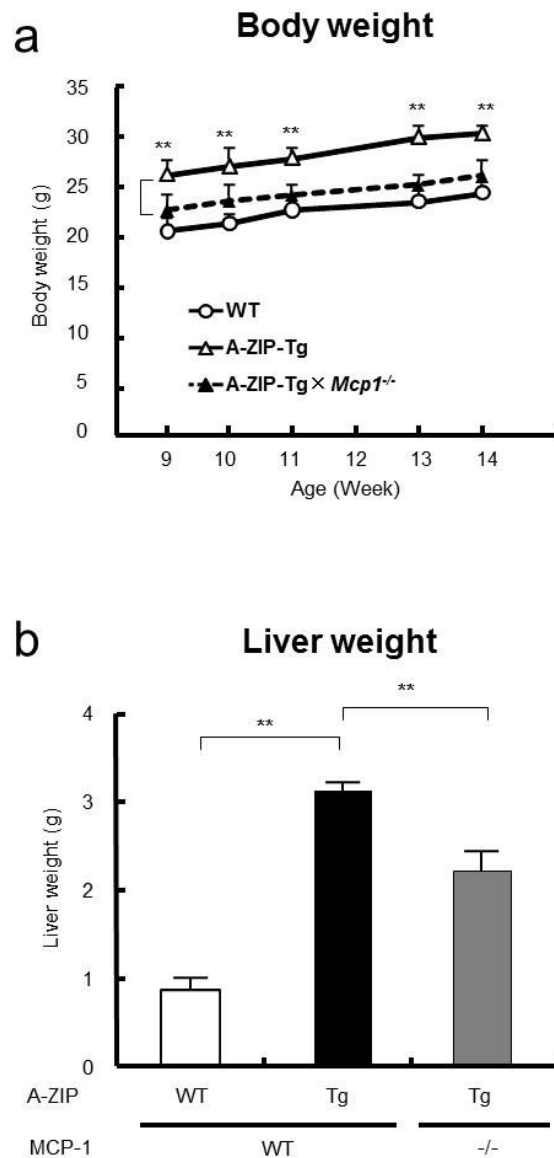
Fig. 5 Body weight and liver weight of WT mice, A-ZIP-Tg mice and A-ZIP-Tg×*Mcp1*$^{-/-}$ mice.

(a) Body weight of WT mice (white circles), A-ZIP-Tg mice (white triangles) and A-ZIP-Tg×*Mcp1*$^{-/-}$ mice (black triangles) were measured from 9 to 14 weeks of age, as indicated. (b) Liver weight of WT (white bars), A-ZIP-Tg (black bars) and A-ZIP-Tg×*Mcp1*$^{-/-}$ (grey bars) in 15-week-old mice. Data are means±SEM. WT mice, *n*=5; A-ZIP-Tg mice, *n*=17; A-ZIP-Tg×*Mcp1*$^{-/-}$ mice, *n*=16. **$p<0.01$ vs A-ZIP-Tg mice

MCP-1 deficiency ameliorated glucose tolerance in lipoatrophic A-ZIP-Tg mice

A-ZIP-Tg×$Mcp1^{-/-}$ mice showed amelioration of hyperglycaemia, hyperinsulinaemia and hypertriacylglycerolaemia compared with A-ZIP-Tg mice (Fig. 6a–c). To further clarify the effects of MCP-1 deficiency in A-ZIP-Tg mice on glucose tolerance and insulin sensitivity, I performed GTTs. Plasma glucose levels and plasma insulin levels during the GTTs were significantly lower in A-ZIP-Tg×$Mcp1^{-/-}$ mice than in A-ZIP-Tg mice (Fig. 6d,e), suggesting that MCP-1 deficiency in A-ZIP-Tg mice partially ameliorated glucose intolerance. In WT mice, plasma insulin levels were increased after glucose administration, whereas they were remarkably decreased in A-ZIP-Tg and A-ZIP-Tg- $Mcp1^{-/-}$ mice, consistent with previous observations that prolonged hyperinsulinaemia due to severe insulin resistance can result in decreased glucose-stimulated insulin-secretion, in particular decreased early-phase insulin secretion [36]. A hyperinsulinaemic-euglycaemic clamp study revealed that the glucose infusion rate was significantly increased in A-ZIP-Tg- $Mcp1^{-/-}$ mice compared with A-ZIP-Tg mice (Fig. 7), indicating that disruption of MCP-1 in A-ZIP-Tg mice could ameliorate insulin resistance.
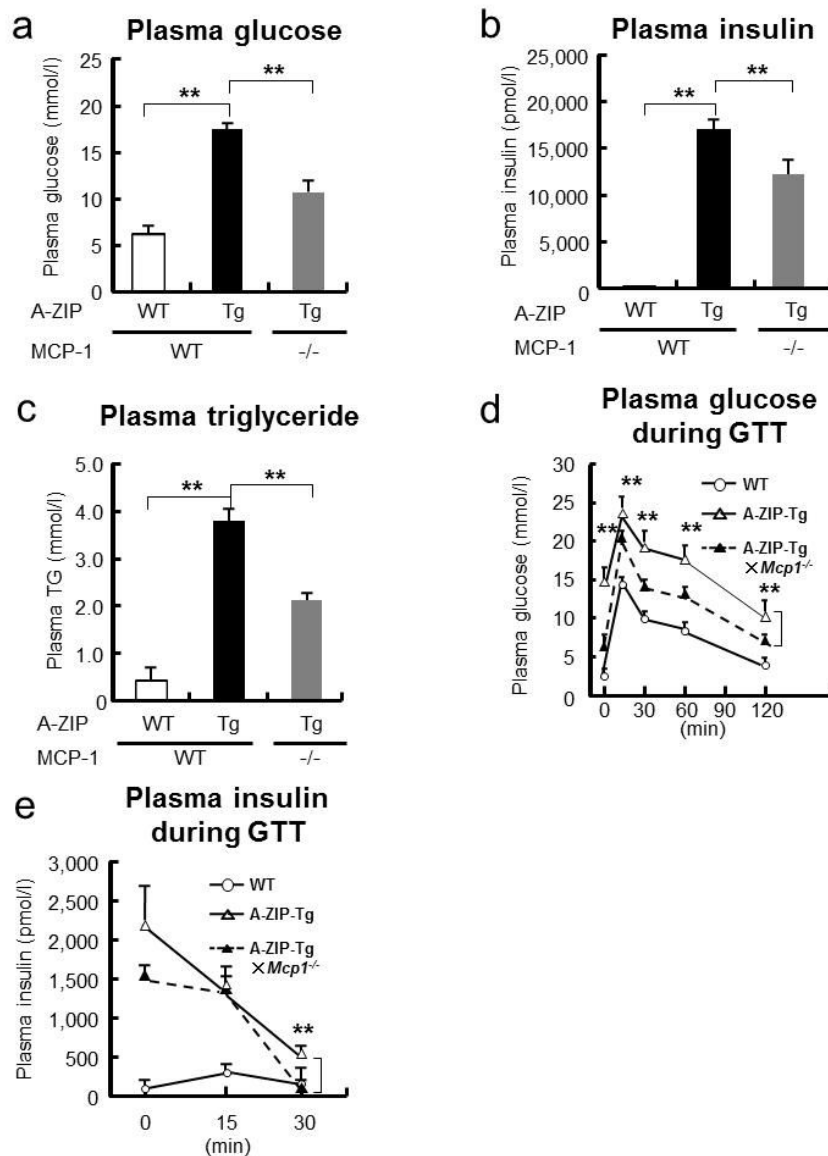
Fig. 6 MCP-1 deficiency in A-ZIP-Tg mice ameliorates glucose intolerance and insulin sensitivity.

Plasma values for glucose (a), insulin (b) and TG (c) were measured in 15-week-old WT (white bars), A-ZIP-Tg (black bars) and A-ZIP-Tg×$Mcp1^{-/-}$ (grey bars) mice. Plasma glucose (d) and plasma insulin (e) during GTT (1.5 g glucose per kilogram body weight) in WT (white circles), A-ZIP-Tg (white triangles) and A-ZIP-Tg×$Mcp1^{-/-}$ (black triangles) in 15-week-old mice. Data are means±SEM. WT mice, n=5; A-ZIP-Tg mice, n=17; A-ZIP-Tg×$Mcp1^{-/-}$ mice, n=16. **p<0.01 vs A-ZIP-Tg mice
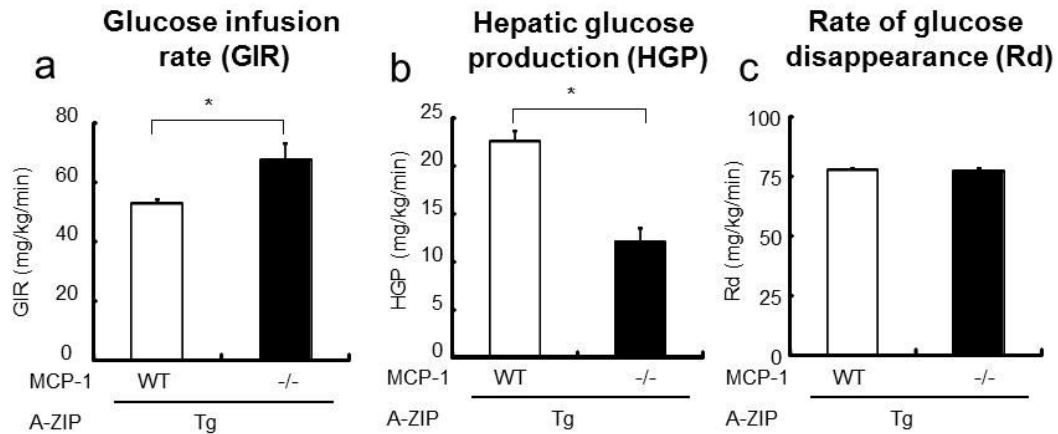
Fig. 7 Hyperinsulinemic-euglycemic clamp study.

Clamp studies were carried out between A-ZIP-Tg mice and A-ZIP-Tg- $Mcp1^{-/-}$ mice. Data represent means±SEM (n=3 per group).*P<0.05 vs A-ZIP-Tg mice. 2-3 days before the study, an infusion catheter was inserted into the right jugular vein under general anesthesia with sodium pentobarbital. Studies were performed on mice under conscious and unstressed conditions after a 6-h fast. A primed continuous infusion of insulin (Humalin R, Lilly) was given (5.0 mill units/g/min), and the blood glucose concentration, monitored every 5 min, was maintained at 11 (mmol/l) by administration of glucose (5g of glucose per 10 mL enriched to 20% with [6,6-^{2}H2] glucose (Sigma)) for 120 min. Blood was sampled via tail tip bleeds at 90, 105, and 120 min for determination of exogenous glucose infusion rates (GIR) (a), hepatic glucose production (HGP) (b) and rate of glucose disappearance (Rd) (c).

Livers from A-ZIP-Tg×Mcp1⁻ᐟ⁻ mice did not decrease the expression of macrophage marker genes in liver, SKM , BAT and also did not reduce of the number of macrophages in liver.

Many studies have demonstrated that macrophage infiltration and levels of proinflammatory cytokines such as MCP-1 and TNF-α are increased in WAT of human obese individuals and several models of rodent obesity [37, 38]. I examined whether the expression of macrophage marker genes would be elevated in other tissues than WAT, such as liver, SKM and BAT, in A-ZIP-Tg mice. The mRNA expressions of *Mcp-1*, *Mcp-3* (*Ccl7*), *Ccr2*, *Emr1* (EGF-like module containing, mucin-like, hormone receptor-like 1*)* and *Cd68* (CD68 antigen) were increased in the liver (Fig. 8a–e), SKM (Fig. 10a-e) and BAT (Fig. 11a-e) of A-ZIP-Tg mice compared with WT mice. The mRNA expressions of *Mcp-2* were significantly increased in the liver and BAT of A-ZIP-Tg mice compared with those of WT mice. MCP-1 deficiency did not significantly decrease the expressions of *Mcp-2* in the liver, SKM and BAT in A-ZIP-Tg mice (Fig. 12). Next, I conducted 1-OH staining for detection of the actual number of macrophages in liver [28]. Same as gene expression data, actually, the number of 1-OH staining positive macrophages were increased in liver from A-ZIP-Tg mice but it did not decreased in MCP-1 deficient A-ZIP-Tg mice (Fig. 9)

Livers from A-ZIP-Tg×Mcp1$^{-/-}$ mice showed increased markers of alternatively activated M2 macrophages

Unexpectedly, MCP-1 deficiency did not decrease the expression of macrophage marker genes in other tissues than WAT, such as the liver, SKM and BAT in A-ZIP-Tg mice. Because a previous report showed that ATMs isolated from obese *Ccr2*-deficient mice expressed alternatively activated M2-macrophage markers [14], I hypothesised that livers from A-ZIP-Tg×*Mcp1*$^{-/-}$ mice might contain M2-polarised macrophages more abundantly. Interestingly, characteristic M2-macrophage marker genes such as *Chi3l3*, *Arg1* and *Tgfb1* were significantly increased in livers from A-ZIP-Tg×*Mcp1*$^{-/-}$ mice (Fig. 8f–h). In contrast to liver, characteristic M2-macrophage marker genes such as *Chi3l3, Arg1* and *Tgfb1* were not significantly changed in SKM and BAT from A-ZIP-Tg×*Mcp1*$^{-/-}$ mice (Fig. 10, 11f-h). Thus, MCP-1 deficiency did not reduce macrophage markers but rather induced macrophages to shift to a M2-polarised state in livers from A-ZIP-Tg mice. These data suggest that MCP-1 deficiency enhances M2 polarisation in livers of A-ZIP-Tg mice.
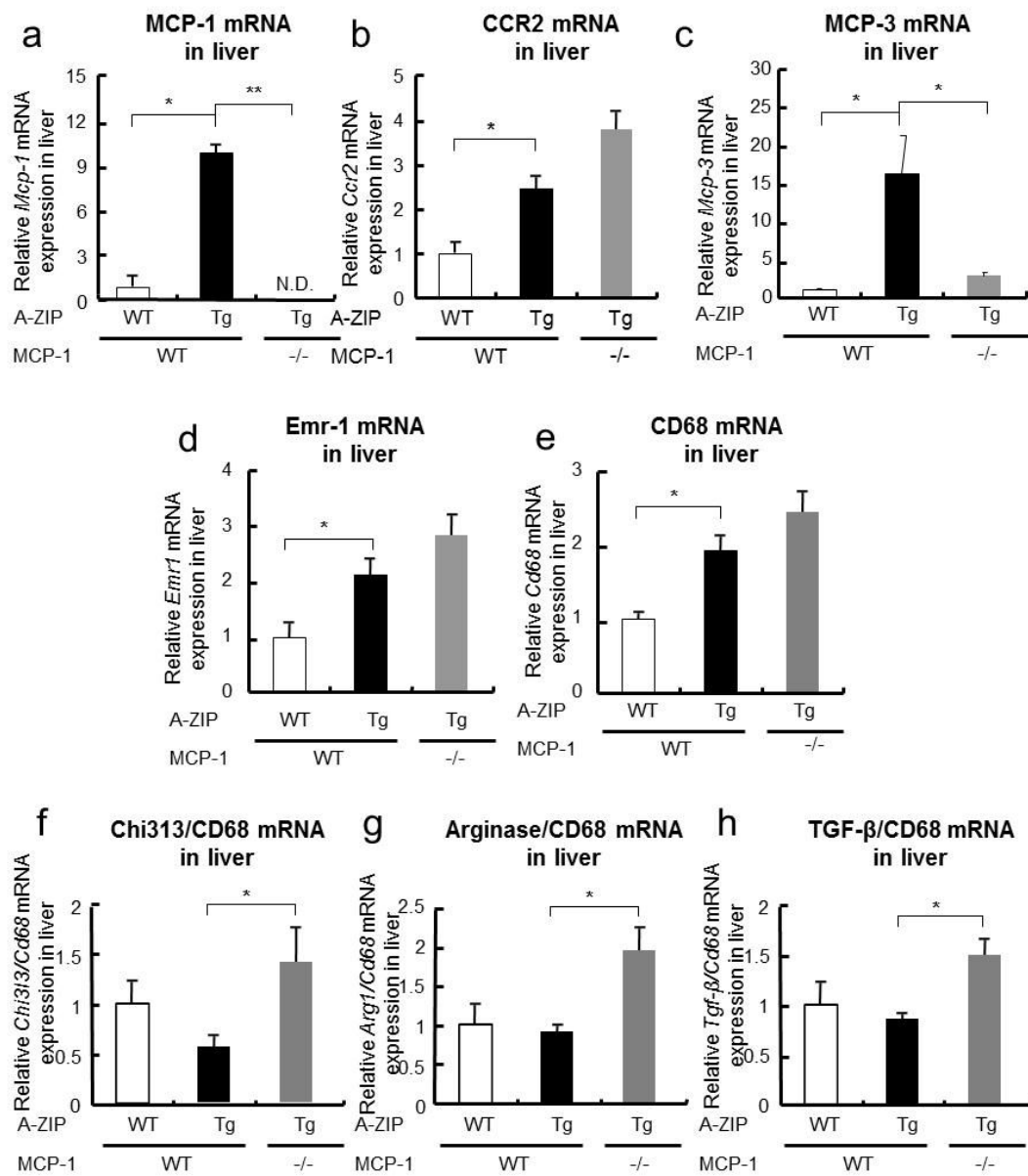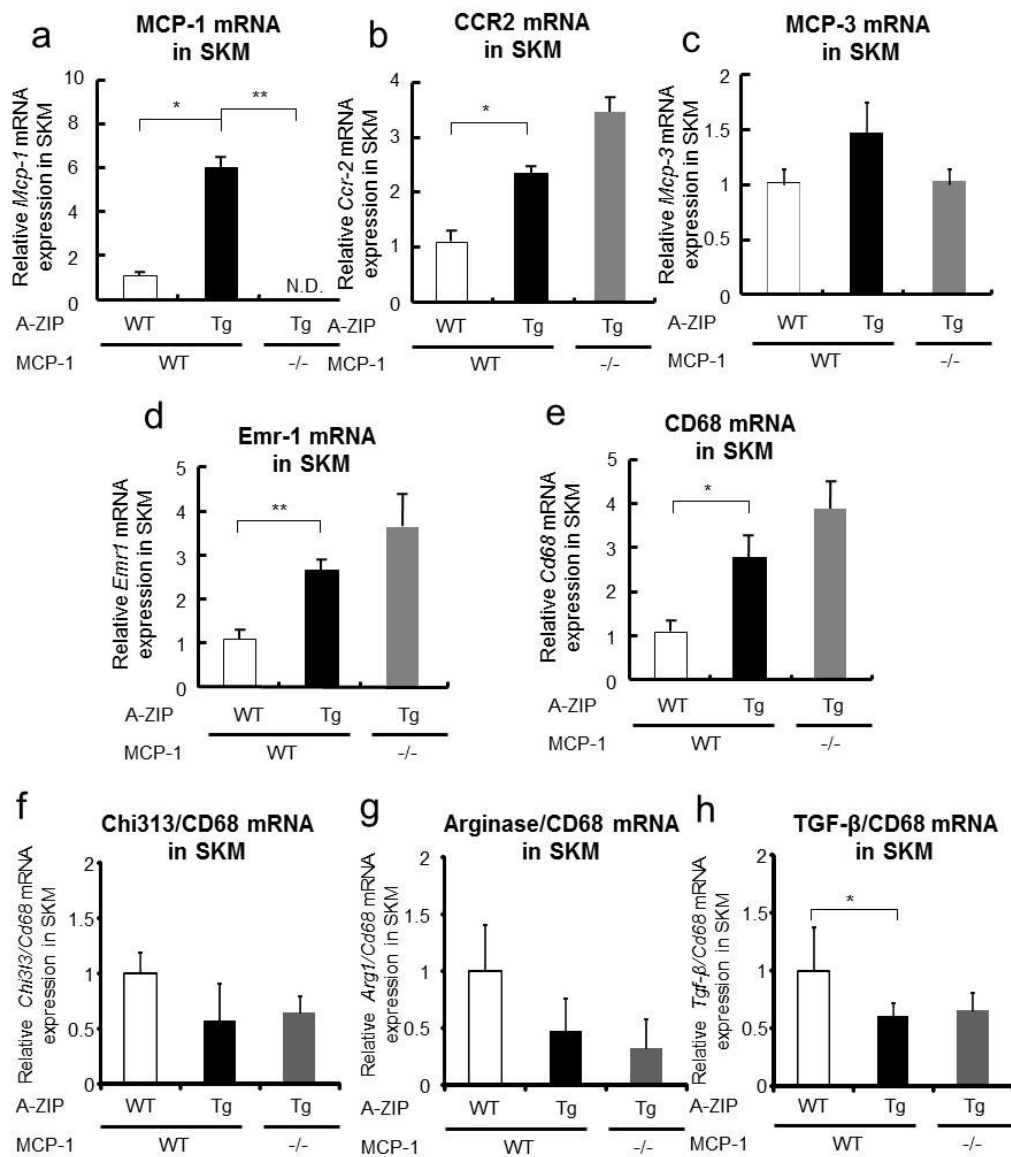
Fig. 8　Effects of MCP-1 deficiency on the expression of macrophage marker genes in liver. *Mcp-1* (a), *Ccr2* (b), *Mcp-3* (c), *Emr1* (d) and *Cd68* (e) mRNA levels and the mRNA ratio of *Chi3l3/Cd68* (f), *Arg1/Cd68* (g) and *Tgf-β/Cd68* (h) in livers from WT (white bars), A-ZIP-Tg (black bars) and A-ZIP-Tg×*Mcp1*$^{-/-}$ (grey bars) in 15-week-old mice in the fed state were analysed by real-time quantitative PCR. Data are means±SEM. WT mice, *n*=5; A-ZIP-Tg mice, *n*=17; A-ZIP-Tg×*Mcp1*$^{-/-}$ mice, *n*=16. *p<0.05 vs A-ZIP-Tg mice

Macrophage staining in liver (Hem-oxygenase staining)

WT   A-ZIP-Tg   A-ZIP-Tg × *Mcp1⁻ᐟ⁻*
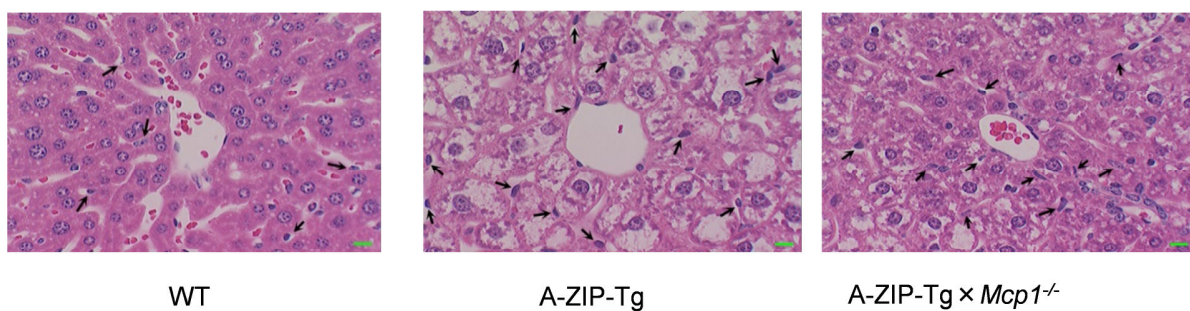
Fig. 9 Macrophage staining in liver.

Livers from WT mice, A-ZIP-Tg mice and A-ZIP-Tg×*Mcp1*$^{-/-}$ mice were fixed overnight in 10% formalin (vol./vol.). Samples were routinely embedded in paraffin. Approximately 5 μm-thick slices obtained from these liver samples were stained with anti-hem-oxygenase-1 (HO-1). Representative sections of livers were stained with HO-1 (Scale bars, 100 μm) from WT, A-ZIP-Tg and A-ZIP-Tg×*Mcp1*$^{-/-}$ in 15-week-old mice.
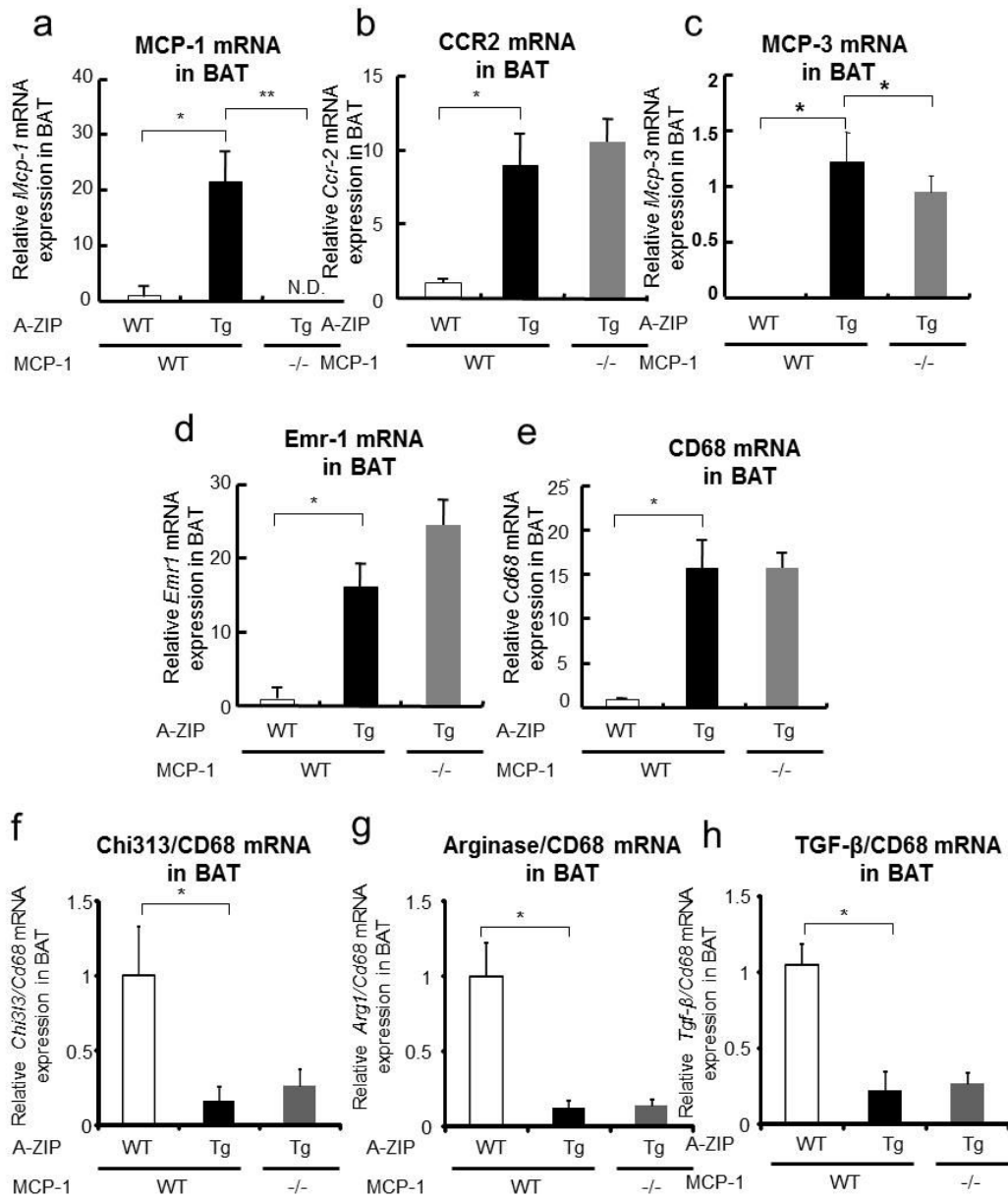
Fig. 10 Effects of MCP-1 deficiency on the expression of macrophage marker genes in SKM. *Mcp-1* (a), *Ccr2* (b), *Mcp-3* (c), *Emr1* (d), *Cd68* (e) mRNA levels and the mRNA ratio of *Chi3l3/Cd68* (f), *Arg1/Cd68* (g) and *TGF-β/Cd68* (h) in SKM in 15-week-old WT (white bars), A-ZIP-Tg (black bars), and A-ZIP transgenic MCP-1 knockout (A-ZIP-Tg×*Mcp1*$^{-/-}$) (grey bars) mice in the fed state were analyzed by real-time quantitative PCR. Data represent means±SEM (WT mice, *n*=5; *Mcp1*$^{-/-}$ mice, *n*=5).*P<0.05, **P<0.01 vs A-ZIP-Tg mice.

Fig. 11 Effects of MCP-1 deficiency on the expression of macrophage marker genes in BAT. *Mcp-1* (a), *Ccr2* (b), *Mcp-3* (c), *Emr1* (d), *Cd68* (e) mRNA levels and the mRNA ratio of *Chi3l3/Cd68* (f), *Arg1/Cd68* (g) and *TGF-β/Cd68* (h) in BAT in 15-week-old WT (white bars), A-ZIP-Tg (black bars), and A-ZIP transgenic MCP-1 knockout (A-ZIP-Tg×*Mcp1*$^{-/-}$) (grey bars) mice in the fed state were analyzed by real-time quantitative PCR. Data represent means±SEM (WT mice, *n*=5; *Mcp1*$^{-/-}$ mice, *n*=5).*P<0.05, **P<0.01 vs A-ZIP-Tg mice.
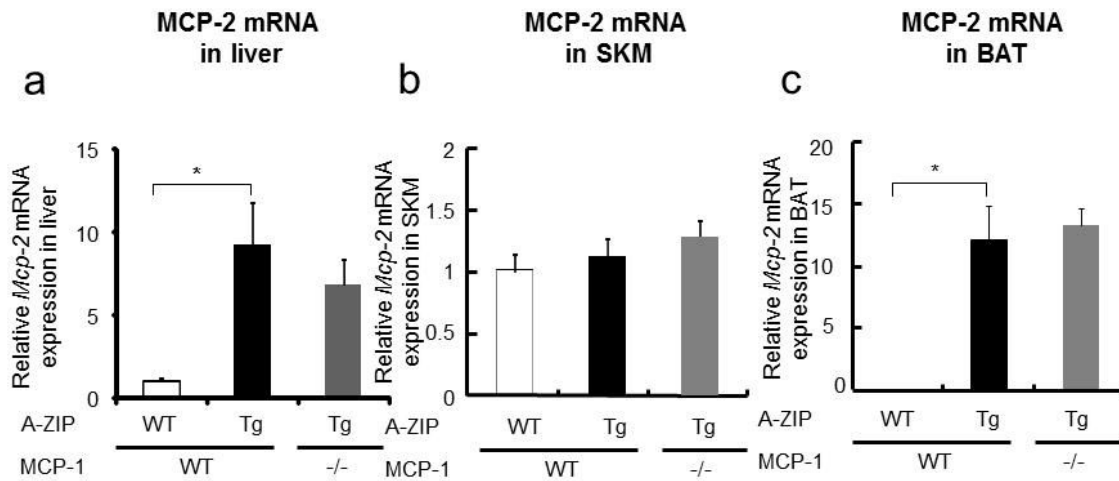
Fig. 12 Effects of MCP-1 deficiency on the expression of MCP-2 gene expessions in liver, SKM and BAT.

Mcp-2 mRNA levels in liver (a), SKM (b) and BAT (c) from WT (white bars), A-ZIP-Tg (black bars) and A-ZIP-Tg×*Mcp1*$^{-/-}$ (grey bars) in 15-week-old mice in the fed state were analyzed by real-time quantitative PCR. Data represent means±SEM (WT mice, *n*=5; A-ZIP-Tg mice, *n*=17 and A-ZIP-Tg×*Mcp1*$^{-/-}$ mice, *n*=16). *P<0.05 vs A-ZIP-Tg mice.

MCP-1 deficiency decreased liver TG content in A-ZIP-Tg mice

It was previously reported that A-ZIP-Tg mice showed dyslipidaemia and severe hepatic steatosis [18]. Liver weights were markedly reduced in A-ZIP-Tg×*Mcp1*$^{-/-}$ mice compared with A-ZIP-Tg mice (Fig. 5b). Representative histological sections of livers showed that MCP-1 deficiency decreased TG accumulation (Fig. 13a). I subsequently determined that the TG content in livers from A-ZIP-Tg×*Mcp1*$^{-/-}$ mice was significantly less than that in livers from A-ZIP-Tg mice (Fig. 13b). To clarify the mechanism by which hepatic steatosis was improved, I studied the expression of genes involved in lipid and energy metabolism and found that expression of *Ppara* mRNA tended to be increased and expression of genes involved in energy dissipation such as *Ucp2* significantly increased in A-ZIP-Tg- *Mcp1*$^{-/-}$ mice compared with A-ZIP-Tg mice, whereas the expression of genes involved in lipogenesis such as *Srebp-1c* (*Srebf1*) and *Scd-1* was not significantly changed (Fig. 14).
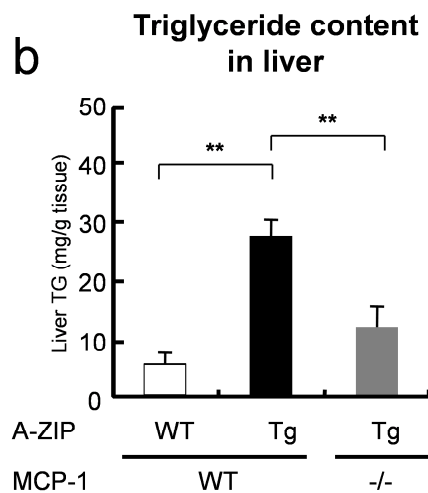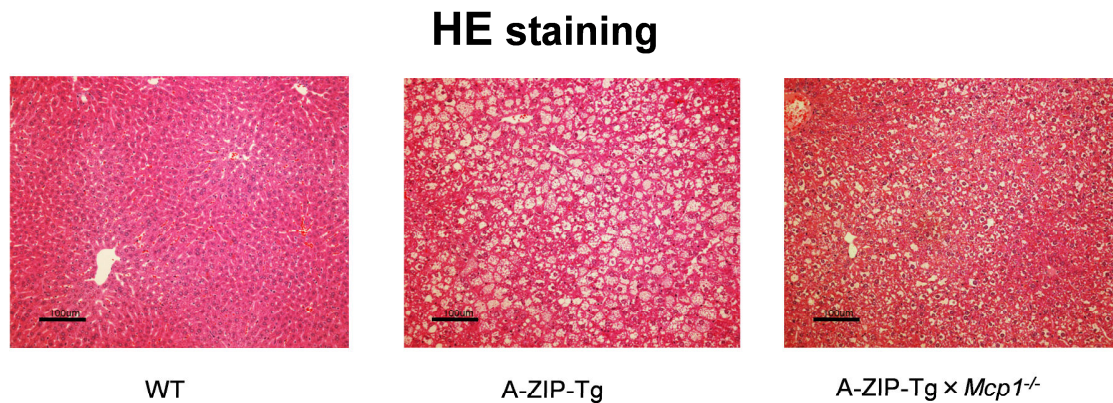
HE staining

WT   A-ZIP-Tg   A-ZIP-Tg × *Mcp1*$^{-/-}$

b **Triglyceride content in liver**

Fig. 13 Histological analysis and TG content of liver.

(a) Sections of livers were stained with haematoxylin and eosin (Scale bars, 100 μm). (b) TG content of livers from WT (white bars), A-ZIP-Tg (black bars) and A-ZIP-Tg×*Mcp1*$^{-/-}$ (grey bars) mice. Data are means±SEM. WT mice, $n=5$; A-ZIP-Tg mice, $n=17$; A-ZIP-Tg×*Mcp1*$^{-/-}$ mice, $n=16$. **$p<0.01$ vs A-ZIP-Tg mice
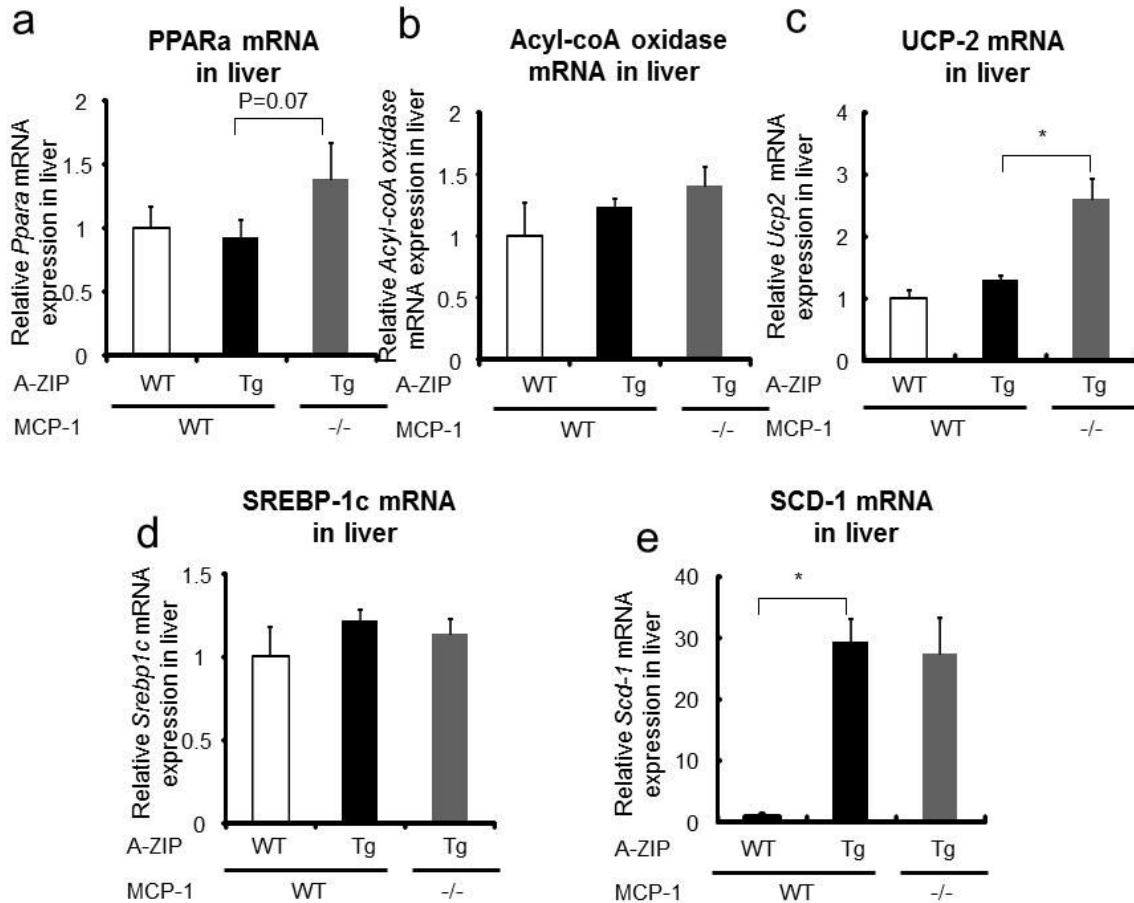
Fig. 14 Effects of MCP-1 deficiency on the expression of genes involved in fatty acid oxidation and synthesis in liver.

Ppara (a), *Acyl-coA oxidase* (b), *Ucp-2* (c), *Srebp-1c* (d) and *Scd-1* (e) mRNA levels in livers from WT (white bars), A-ZIP-Tg (black bars) and A-ZIP-Tg×*Mcp1*$^{-/-}$ (grey bars) in 15-week-old mice in the fed state were analyzed by real-time quantitative PCR. Data represent means±SEM (WT mice, n=5; A-ZIP-Tg mice, n=17 and A-ZIP-Tg×*Mcp1*$^{-/-}$ mice, n=16). *P<0.05 vs A-ZIP-Tg mice.

MCP-1 deficiency enhanced insulin signalling in livers of A-ZIP-Tg mice

Previous studies have reported that MCP-1 induces phosphorylation of ERK through activation of CCR2 in SKM, myocytes, kidney and leukaemia cells [9, 10, 39, 40]. Moreover, Bost et al reported that mice lacking ERK-1 were protected from high-fat diet-induced obesity and insulin resistance [41]. Thus, I hypothesised that inhibition of ERK signalling would improve insulin signalling in A-ZIP-Tg mice, so I studied phosphorylation of ERK-1/2 in livers from A-ZIP-Tg mice and A-ZIP-Tg×$Mcp1^{-/-}$ mice. In fact, ERK-1/2 and p38MAPK phosphorylation were significantly increased in livers from A-ZIP-Tg mice compared with WT mice. Conversely, phosphorylation of ERK-1/2 was decreased in livers from A-ZIP-Tg×$Mcp1^{-/-}$ mice compared with A-ZIP-Tg mice (Fig. 15a). I next examined the effects of MCP-1 deficiency on insulin signalling in livers from A-ZIP-Tg mice. In livers from A-ZIP-Tg×$Mcp1^{-/-}$ mice, tyrosine phosphorylation of IR-β and serine phosphorylation of Akt were significantly increased compared with that seen in A-ZIP-Tg mice (Fig. 16). Moreover, Ser 612 in IRS-1 has been reported to be phosphorylated by ERK [41], which would result in inhibition of insulin signalling. The amount of Ser 612 phosphorylation in IRS-1 was significantly decreased in livers from A-ZIP-Tg×$Mcp1^{-/-}$ mice compared with A-ZIP-Tg mice (Fig. 17). Furthermore, in SKM from A-ZIP-Tg×$Mcp1^{-/-}$ mice, tyrosine phosphorylation of

IR-β was significantly, and serine phosphorylation of Akt tended to be, increased compared
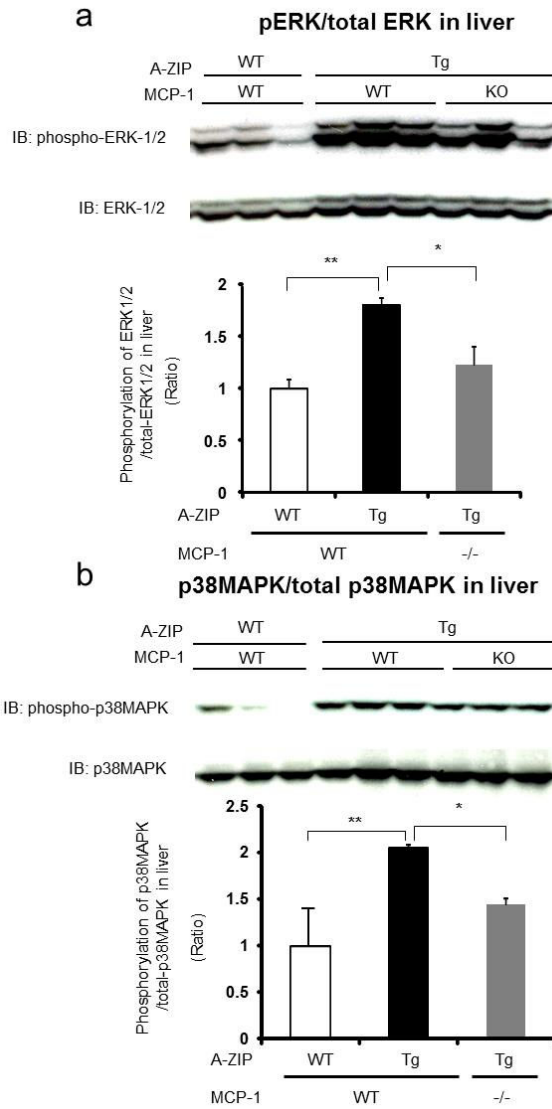
with A-ZIP-Tg mice (Fig. 18).

Fig. 15 MCP-1 deficiency in livers from A-ZIP-Tg mice results in the phosphorylation of ERK-1/2 and p38MAPK.

Phosphorylation of ERK1/2 (a) and p38MAPK (b) in livers from WT, A-ZIP-Tg and A-ZIP-Tg×Mcp1$^{-/-}$ 15-week-old mice in the fed state were analysed by immunoblotting. The relative amount of each protein was normalised to the total amount of ERK-1/2 or p38MAPK and the ratio is shown. Data are means±SEM (n=3 per group). *p<0.05, **p<0.01 vs WT or A-ZIP-Tg mice.
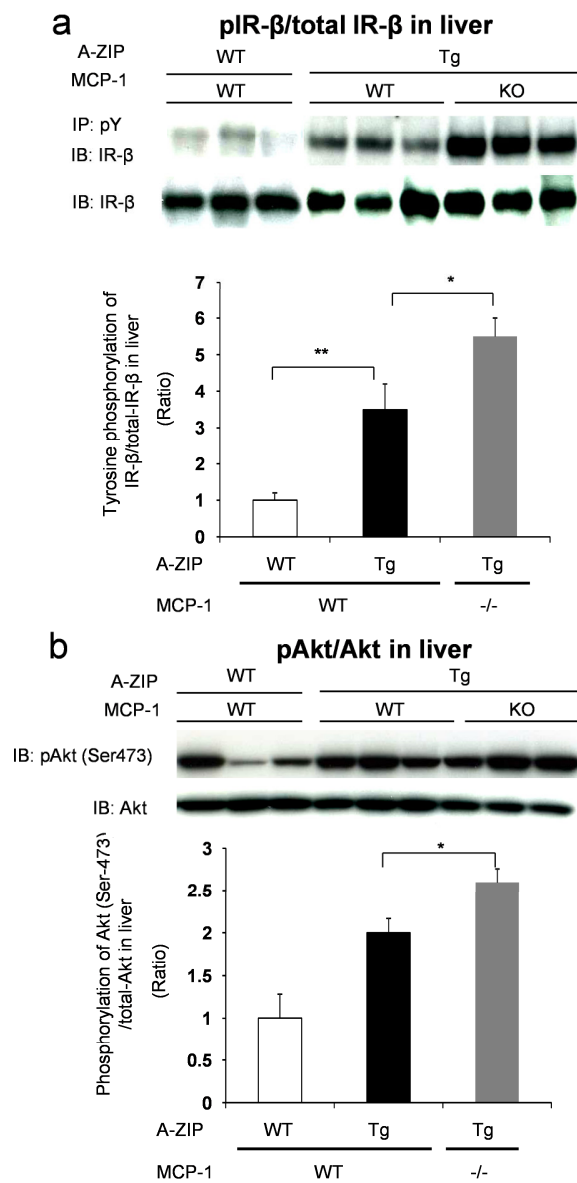
46

Fig. 16 MCP-1 deficiency in livers from A-ZIP-Tg mice results in increased insulin signalling.

Tyrosine phosphorylation of IR-β (a) and phosphorylation of Akt (Ser-473) (b) in livers from WT, A-ZIP-Tg and A-ZIP-Tg×$Mcp1^{-/-}$ 15-week-old mice in the fed state were analysed by immunoblotting. The relative amount of each protein was normalised to the total amount of IR-β or Akt and the ratio is shown. Data are means±SEM (n=3 per group). *p<0.05, **p<0.01 vs WT or A-ZIP-Tg mice
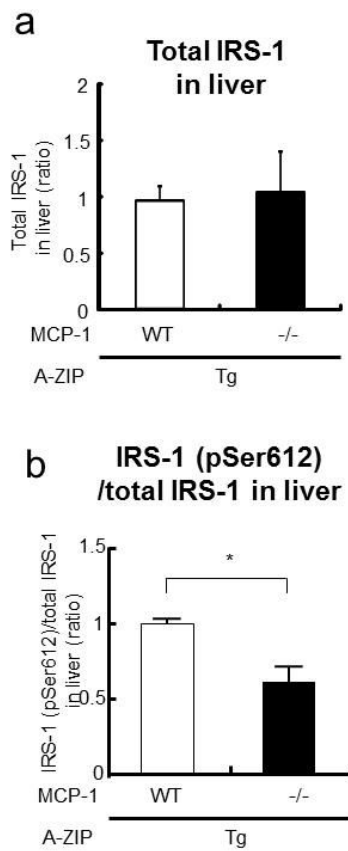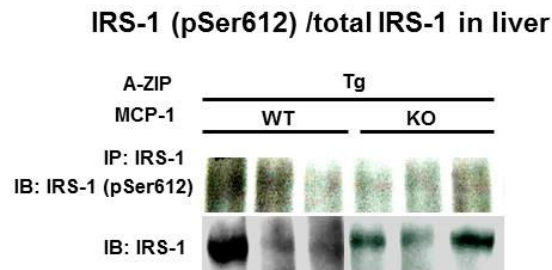
Fig. 17 MCP-1 deficiency in livers from A-ZIP-Tg mice results in the phosphorylation of Ser-612 of IRS-1.

Total amount of IRS-1 (a) and phosphorylation of Ser-612 in IRS-1 (b) in livers from A-ZIP-Tg (white bars) and A-ZIP-Tg×$Mcp1^{-/-}$ (black bars) 15-week-old mice in the fed state were analyzed by immunoprecipitation. The relative amount of each protein was normalized to the total amount of IRS-1. Data represent means ± S.E.M. ($n = 3$ per group).* $P < 0.05$ versus A-ZIP-Tg mice.
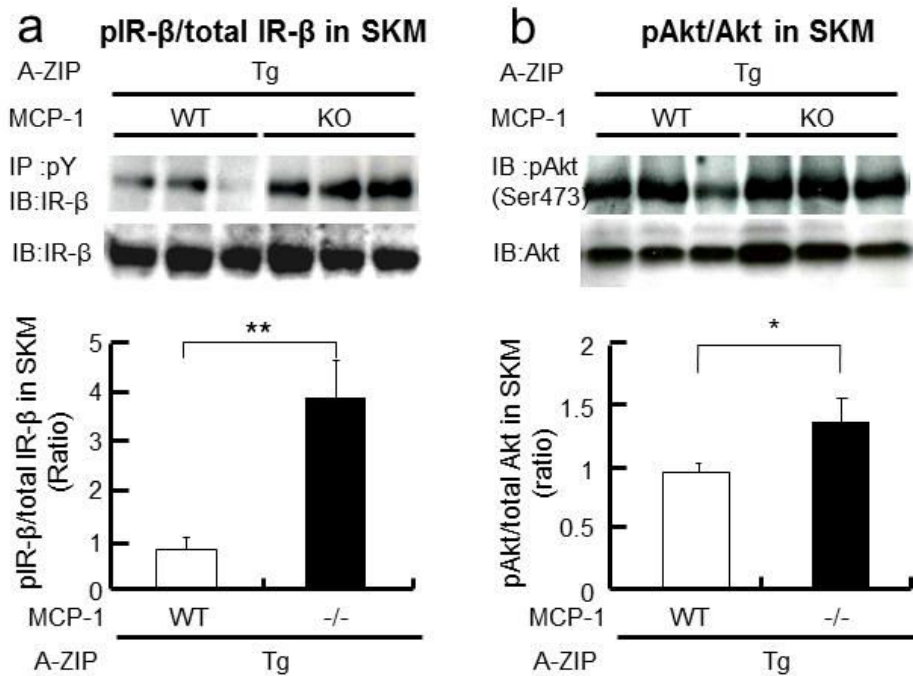
Fig. 18 MCP-1 deficiency in SKM from A-ZIP-Tg mice results in increased insulin signaling.
Tyrosine phosphorylation of IR-β (a) and phosphorylation of Akt (Ser-473) (b) in SKM from
A-ZIP-Tg (white bars) and A-ZIP-Tg×Mcp1$^{-/-}$(black bars) 15-week-old mice in the fed state
were analyzed by immunoblotting. The relative amount of each protein was normalized to the
total amount of IR-β or Akt. Data represent means±SEM (n=3 per group).*$P<0.05$, **$P<0.01$ vs
A-ZIP-Tg mice.

MCP-1 deficiency decreased islet hypertrophy and increased insulin staining positive cells.

Representative histological sections of islets showed that MCP-1 deficiency in A-ZIP-Tg mice decreased islet hypertrophy and increased insulin staining positive cells in islet (Fig. 19). These results would lead to improvement of glucose-stimulated insulin secretion of MCP-1 deficient A-ZIP-Tg mice in OGTT (Fig. 6e).
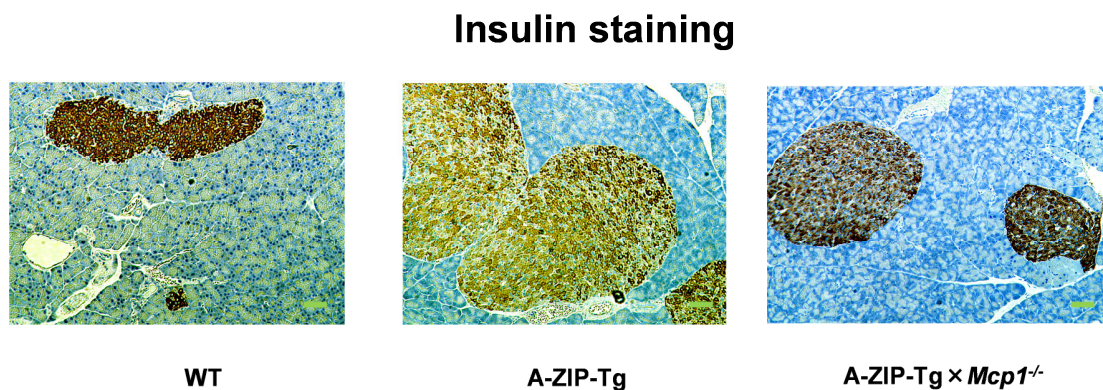
Insulin staining

WT　　　　　　　A-ZIP-Tg　　　　　A-ZIP-Tg × *Mcp1*$^{-/-}$

Fig. 19 MCP-1 deficiency decreased islet hypertrophy and increased insulin staining positive cells in A-ZIP-Tg mice.

Islets from WT mice, *Mcp1*$^{-/-}$ mice, A-ZIP-Tg mice and A-ZIP-Tg×*Mcp1*$^{-/-}$ mice were fixed overnight in 10% formalin (vol./vol.). Samples were routinely embedded in paraffin. Approximately 5 μm-thick slices obtained from these islet samples were stained with anti-insulin antibody. Representative sections of islets were stained with anti-insulin antibody (Scale bars, 100 μm) from WT mice, A-ZIP-Tg mice and A-ZIP-Tg×*Mcp1*$^{-/-}$ mice.

Improvement of atherosclerosis in MCP-1 deficient A-ZIP-Tg mice.

Previous study showed that CCR2 deficient mice reduced atherosclerosis in cuff injured mice (19). Interestingly, although neo intimal formation in aorta of A-ZIP-Tg mice was increased, MCP-1 deficient A-ZIP-Tg mice significantly reduced it. (Fig. 20). These results suggest that MCP-1 deficiency could atherosclerosis in lipoatrophy patients.

Neo intimal formation of the femoral arteries
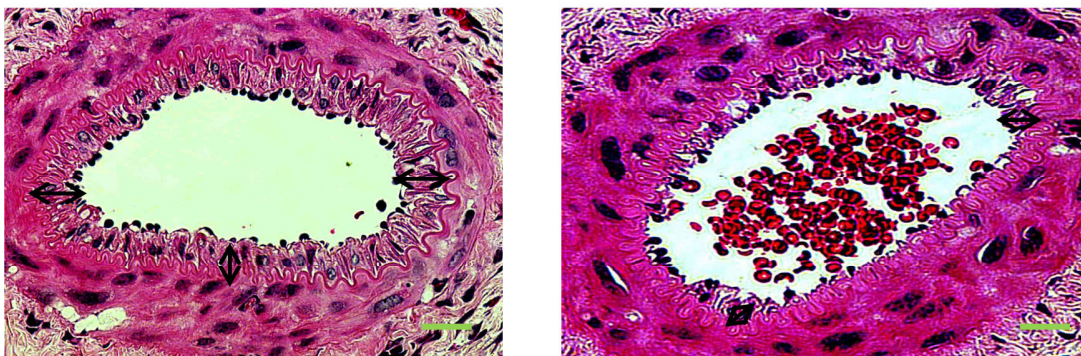
A-ZIP-Tg   **A-ZIP-Tg × Mcp1⁻/⁻**

Fig. 20 MCP-1 deficiency showed decreased neo intimal formation in A-ZIP-Tg mice.
2 weeks after cuff placement, vessels were foxed with 10% formalin and embedded in paraffin. Continuous cross-sections of the femoral arteries from A-ZIP-Tg mice and A-ZIP-Tg×$Mcp1^{-/-}$ mice were cut from one end of the cuffed portion to the other end and were stained for elastic fibers and with hematoxylin and eosin. The thickness of the neo intimal formation was observed by digital microscope camera. (Black arrows shows the lesions of neo intimal formation) (Scale bars, 100 μm)

DISCUSSION

MCP-1/CCL2 secreted from WAT in obesity has been reported to contribute to tissue macrophage accumulation and insulin resistance by inducing a chronic inflammatory state. MCP-1, CCR2 and M1 macrophage marker genes have been shown to be elevated in the fatty liver of lipoatrophic A-ZIP-Tg mice. In addition, phosphorylation of ERK1/2 and p38MAPK, *Scd1* and *Acc1* mRNA which contribute to fatty acid synthesis are also increased in the fatty liver of A-ZIP-Tg mice (Fig. 21-1). Though I could not identify the source of the induction of MCP-1 in the fatty liver of A-ZIP-Tg mice, there is some potential that increase of endogenous macrophage infusion such as Kupffer cells could produce MCP-1 in the liver of A-ZIP-Tg mice (Fig. 9). Moreover, Mandrekar et al showed that hepatocytes as well as Kupffer cells expressed high amounts of MCP-1 mRNA in the liver of alcohol induced liver injury with steatosis [35]. Thus, not only endogenous macrophage but also hepatocytes would be the main candidates for overproduction of MCP-1 in the liver of A-ZIP-Tg mice. Treatment of these mice with CCR2 antagonist has been shown to ameliorate their hyperglycaemia, hyperinsulinaemia and hepatomegaly, in conjunction with a reduction in liver inflammation. However, since CCR2 antagonist can block not only MCP-1, but also MCP-2 and MCP-3, it remains unclear whether

MCP-1 secreted from liver could contribute to hyperglycaemia, hyperinsulinaemia and hepatomegaly in conjunction with liver inflammation, as well as to M1/M2 polarisation. To address these issues, I analyzed the effects of targeted disruption of MCP-1 in A-ZIP-Tg mice. The insulin-sensitive phenotype of A-ZIP-Tg- $Mcp1^{-/-}$ mice was prominent in female mice compared with male mice. It was reported that lipoatrophy associated features include polycyctic ovary syndrome in woman [42]. Polycystic ovary syndrome shows excessive amounts of androgenic hormons, resulting in insulin resistance, often associated with type 2 diabetes. Though I did not analyzed, lipoatrophic A-ZIP-Tg mice might show polycystic ovary syndrome, which leads to worsen insulin sensitivity. In addition, northern blotting study showed MCP-1 was also expressed in the ovary of A-ZIP-Tg mice. Thus, ovariectomy may ameliorate insulin resistance of female A-ZIP-Tg mice by blocking MCP-1 excretion from ovary. Due to these ovary disorder and MCP-1 expression from ovary might lead to the gender difference of insulin resistance of MCP-1 deficient A-ZIP-Tg mice. Furthermore, in other cytokine deficient mice, CXC motif chemokine ligand-14 (CXCL-14) mice, the insulin-sensitive phenotype after high fat diet feeding was also prominent in female mice but not in male mice [43]. These gender difference of cytokine deficient mice for insulin resistance might be important for the future study.   In the current study, I showed for the first time that

targeted disruption of MCP-1 alone in lipoatrophic diabetic A-ZIP-Tg mice ameliorated insulin

resistance and hepatic steatosis, which was associated with decreased ERK-1/2 and p38MAPK

phosphorylation (Fig. 15) and alternative M2 activation of macrophages. However, MCP-1

deficient A-ZIP-Tg mice also decreased MCP-3 mRNA expression in liver and BAT. MCP-3 is

located on chromosome 11 in mice and   most closely related to MCP-1, MCP-1 is also located

in chromosome 11. Thus, reduction of MCP-3 mRNA might be due to transcriptional affect of

MCP-1 gene deletion. There are few reports of MCP-3 for insulin resistance and diabetes as

compared with those of MCP-1. MCP-3 mRNA was reported to be increase in adipose tissue of

obese mice and kidney of type 1 diabetes patients. MCP-3 protein was also increased in urine of

type 1 diabetes patients with long term renal inflammation [44]. Although both MCP-1 and

MCP-3 attract monocytes and regulate macrophage function, besides MCP-3, MCP-1 induces

amylin expression through activation of ERK signaling pathways independent of CCR2.

Increase of amylin contributes to deterioration of insulin resistance [45]. Thus, MCP-1 would

more worsen insulin resistance than MCP-3. In this study, MCP-3 mRNA was not significantly

decreased in SKM of A-ZIP-Tg×$Mcp1^{-/-}$ mice, however, insulin resistance of SKM was

improved as compared with A-ZIP-Tg mice. According to these evidences, the direct effect of

MCP-3 for insulin resistance was not stronger than that of MCP-1. Certainly, though I could not

exclude the effect for the reduction of MCP-3 to insulin resistance, the improvement of insulin

resistance in A-ZIP-Tg×$Mcp1^{-/-}$ mice was assessed to be mainly derived from deficiency of

MCP-1 in A-ZIP Tg mice.

Although food intake was not significantly different when adjusted by body weight (Table

1), daily food intake of A-ZIP-Tg×$Mcp1^{-/-}$ mice was decreased as compared with that of A-ZIP

Tg mice. Thus, pair-feeding, an experimental method in which food intake or energy (calory)

intake are limited to be same between animal groups would be suitable for this study, but I

could not conduct it due to concern of poor longevity of A-ZIP Tg mice. The A-ZIP-Tg mice

with MCP-1 deficiency tended to exhibit increased *Ppara* and exhibited significantly increased

Ucp2 expression in the liver (Fig. 14), raising the possibility that the body weight and liver

weight reduction (Table 2) were due to increased energy expenditure, and that it could also

contribute to the reduction in liver triacylglycerol content. However, it has been technically

extremely difficult to prepare enough A-ZIP-Tg×$Mcp1^{-/-}$ mice to unequivocally prove

increased energy expenditure in these mice. I would like to carry out this experiment in the

future study.

The amounts of tyrosine phosphorylation of IR-β and serine phosphorylation of Akt were

increased in livers from A-ZIP-Tg×$Mcp1^{-/-}$ mice (Fig. 16). These data suggested that the

amelioration of insulin resistance by disruption of MCP-1 in A-ZIP-Tg mice, such as increased

tyrosine phosphorylation of IR-β and serine phosphorylation of Akt in liver, seemed to be

related to decreased ERK-1/2 and p38MAPK activation [46], at least in part.

Although the disruption of MCP-1 in A-ZIP-Tg mice improved insulin resistance, the gene

expression of macrophage markers such as *Emr1* and *Cd68* in the liver were not decreased

compared with those seen in A-ZIP-Tg mice (Fig. 8d,e). It was recently reported that the

induction of M2 markers in resident macrophages in the liver controls hepatic lipid metabolism

[47]. In this study, the M2-specific genes *Chi3l3* and *Arg1* were increased in livers from

A-ZIP-Tg×*Mcp1*$^{-/-}$ mice compared with A-ZIP-Tg mice (Fig. 8f,g). These data are consistent

with the results that ATMs from obese *Ccr2*-deficient mice express M2 markers at levels similar

to those found in lean mice [14]. However, treatment with CCR2 antagonist reduced the

macrophage marker gene *Cd68* mRNA and *Tnf-α* mRNA in the livers of A-ZIP-Tg mice [23].

These results might be derived from differences between a chronic and an acute inhibition of

CCR2 or between targeted disruption of MCP-1 and simultaneous inhibition of

MCP-1/MCP-2/MCP-3 by CCR2 antagonist in the liver of A-ZIP-Tg mice.

Previous studies have shown that CCR2 promoted obesity-induced hepatic steatosis in *db/db*

mice [48], that a CCR2 antagonist (propagermanium) also reduced liver TG content in *db/db*

mice [49], and that another CCR2 antagonist (RS 504393) ameliorated hepatomegaly but did not decrease hepatic TG content significantly (p=0.144) [23]. These results raised the possibility that inhibition of MCP-1 and/or MCP-2 and/or MCP-3 by CCR2 inhibition could be involved in the suppression of hepatic steatosis. In this study, I showed for the first time that targeted disruption of MCP-1 in A-ZIP-Tg mice by itself exhibited decreased liver TG content in the liver (Fig. 13b), clearly indicating that MCP-1 plays an important role in the onset of hepatic steatosis in the liver in A-ZIP-Tg mice.

In terms of treatment for lipoatrophy, leptin-replacement clinical trial by using metreleptin is on-going. However, there are concern about induction of chronic inflammation and emergence of neutralizing antibody for metreleptin. As CCR2 antagonist also prevents inflammation, steatosis and insulin resistance, combination therapy of metreleptin and CCR2 antagonist would bring additive or synergistic effects for amelioration of lipoatrophy.

In conclusion, I showed for the first time that targeted disruption of MCP-1 by itself ameliorated insulin resistance and hepatic steatosis, and at the same time decreased phosphorylation of ERK-1/2 and p38 MAPK (increased tyrosine phosphorylation of IR-β and serine phosphorylation of Akt) and induced alternative M2 activation of macrophages in the fatty liver from lipoatrophic diabetic A-ZIP-Tg mice (Fig. 21-2). These results suggest that

MCP-1 derived from tissues other than WAT, such as fatty liver, could also play an important

role in the regulation of whole body insulin sensitivity, hepatic steatosis, macrophage

polarisation and phosphorylation of ERK-1/2 and p38 MAPK (Fig. 21-3). The current study

also suggests that modulating MCP-1 in the liver would be useful therapy for diabetes and fatty
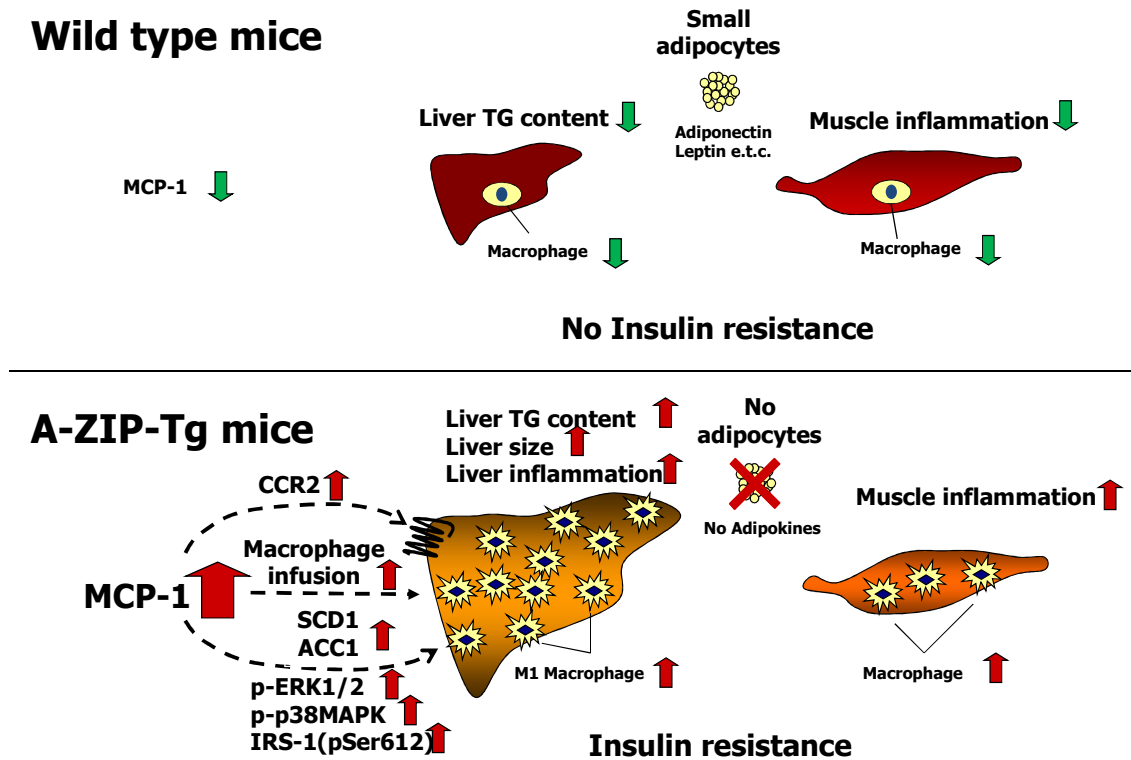
liver.

Fig. 21-1 Phenotypes of A-ZIP transgenic mice as compared with wild-type mice.
Plasma MCP-1 concentrations were significantly increased in A-ZIP-Tg mice and *Mcp-1* mRNA was most abundantly expressed in the liver of A-ZIP-Tg mice. A-ZIP-Tg mice showed liver steatosis, hepatomegaly and increase of M1 macrophage infusion, phosphorylation of ERK, p38MAPK and lipogenic gene expressions such as *Scd1* and *Acc1* mRNA in the liver.
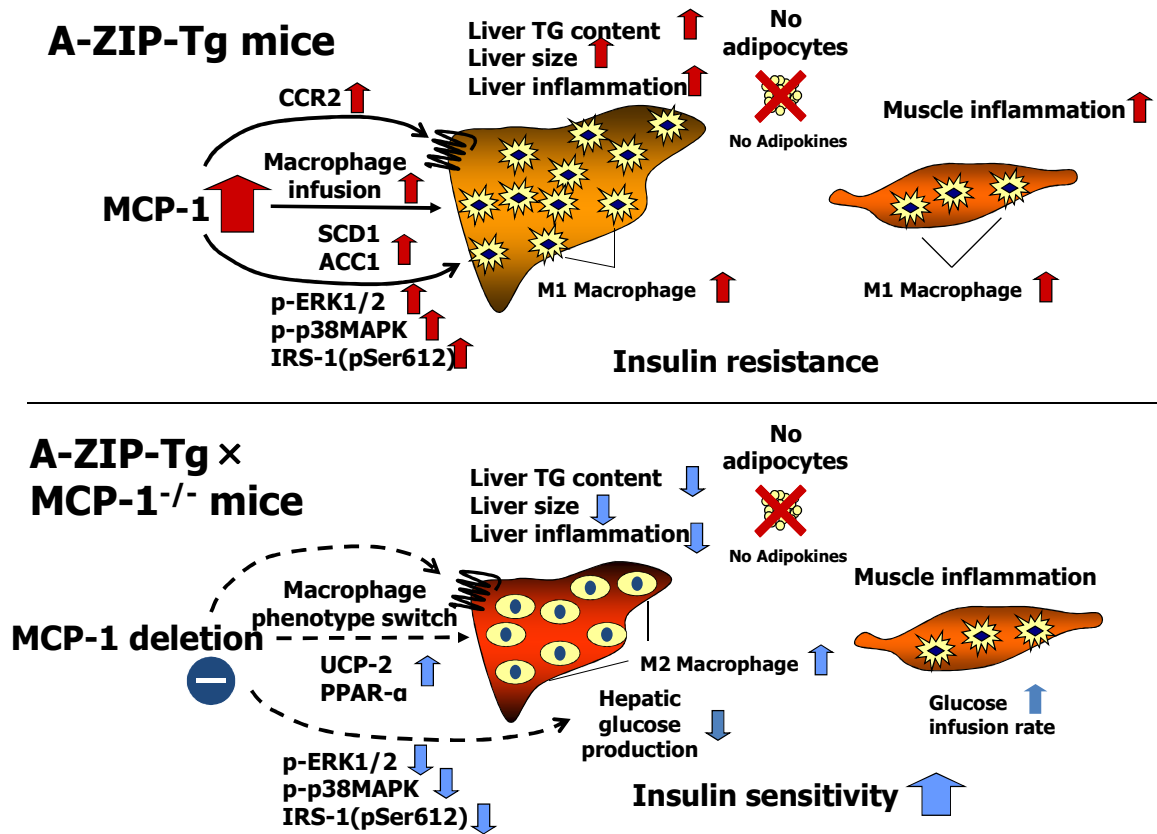
Fig. 22-2 Phenotypes of MCP-1 deficient A-ZIP transgenic mice as compared with A-ZIP transgenic mice.

MCP-1 deficiency ameliorated insulin resistance and hepatic steatosis at the same time decreased phosphorylation of ERK-1/2 and p38MAPK and induced alternative M2 activation of macrophages in the liver of lipoatrophic diabetic A-ZIP-Tg mice. These results suggest that modulating MCP-1 in the liver would be useful therapy for diabetes and hepatic steatosis.
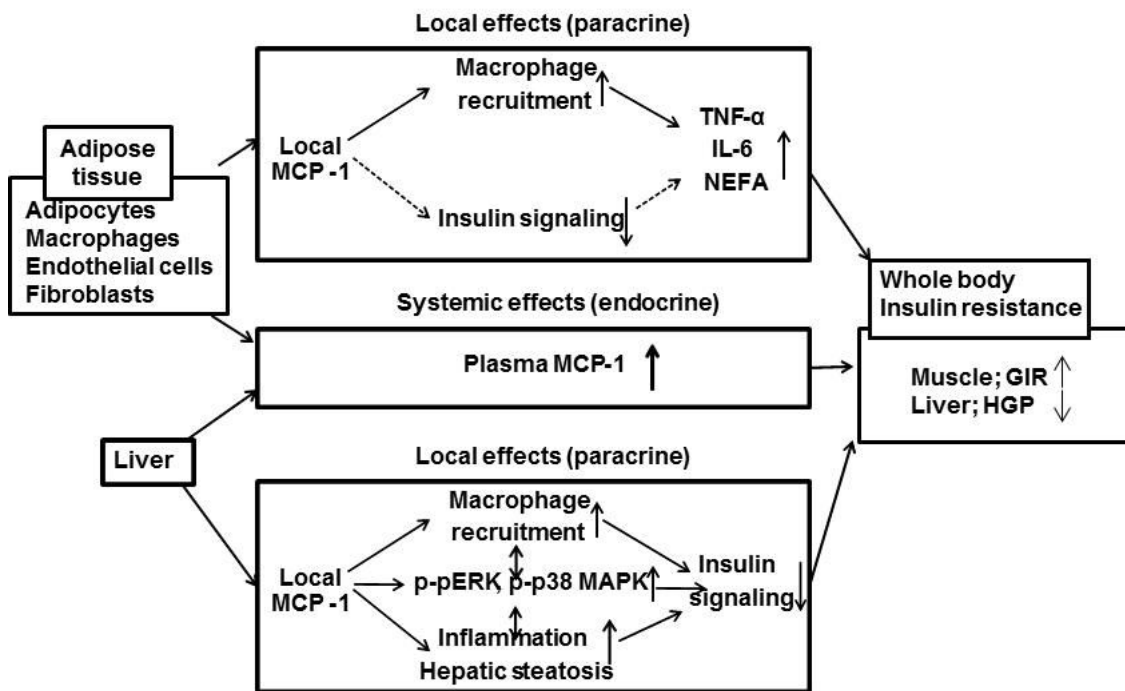
Fig. 22-3 Paracrine and endocrine effects of MCP-1 derived from adipose tissue and liver for whole body insulin resistance.

MCP-1 from adipocytes induce macrophage infiltration and increase insulin resistance causing adipokines. MCP-1 from liver also plays an important role in the regulation of hepatic steatosis, macrophage recruitment and insulin signaling. Both paracrine and endocrine effects of MCP-1from adipocyte and liver could contribute to the development of whole body insulin resistance.

ACKNOWLEDGEMENT

REFERENCES

1. Wellen KE, Hotamisligil GS. Inflammation, stress, and diabetes. *J Clin Invest* 115:1111-1119, 2005

2. Kershaw EE, Flier JS. Adipose tissue as an endocrine organ. *J Clin Endocrinol Metab* 89:2548-2556, 2004

3. Arranz J, Soriano A, Garcia I et al. Effect of proinflammatory cytokines (IL-6, TNF-alpha, IL-1beta) on hemodynamic performance during orthotopic liver transplantation. *Transplant Proc* 35:1884-1887, 2003

4. Xu H, Gosling J, Cleary M et al. Chronic inflammation in fat plays a crucial role in the development of obesity-related insulin resistance. *J Clin Invest* 112:1821-1830, 2003

5. Ito A, Suganami T, Yoshimasa Y et al. Role of MAPK phosphatase-1 in the induction of monocyte chemoattractant protein-1 during the course of adipocyte hyoertrophy *J Biol Chem* 282: 25445-52, 2007

6. Boring L, Gosling J, Cleary M, Charo IF. Decreased lesion formation in CCR2-/- mice reveals a role for chemokines in the initiation of atherosclerosis. *Nature* 394:894-897, 1998

7. Weisberg SP, McCann D, Desai M, Rosenbaum M, Leibel RL, Ferrante AW, Jr. Obesity is associated with macrophage accumulation in adipose tissue. *J Clin Invest* 112:1796-1808,

2003

8. Xu H, Barnes GT, Yang Q et al. Chronic inflammation in fat plays a crucial role in the development of obesity-related insulin resistance. *J Clin Invest* 112:1821-1830, 2003

9. Kamei N, Tobe K, Suzuki R et al. Overexpression of monocyte chemoattractant protein-1 in adipose tissues causes macrophage recruitment and insulin resistance. *J Biol Chem* 281:26602-26614, 2006

10. Jimenez-Sainz MC, Fast B, Mayor F, Jr., Aragay AM. Signaling pathways for monocyte chemoattractant protein 1-mediated extracellular signal-regulated kinase activation. *Mol Pharmacol* 64:773-782, 2003

11. Gordon S, Taylor PR. Monocyte and macrophage heterogeneity. *Nat Rev Immunol* 5:953-964, 2005

12. Mantovani A, Sica A, Sozzani S, Allavena P, Vecchi A, Locati M. The chemokine system in diverse forms of macrophage activation and polarization. *Trends Immunol* 25:677-686, 2004

13. Kanda H, Tateya S, Tamori Y et al. MCP-1 contributes to macrophage infiltration into adipose tissue, insulin resistance, and hepatic steatosis in obesity. *J Clin Invest* 116:1494-1505, 2006

14. Lumeng CN, Bodzin JL, Saltiel AR. Obesity induces a phenotypic switch in adipose tissue

macrophage polarization. *J Clin Invest* 117:175-184, 2007

15. Chou K and Perry CM. Metreleptin: first global approval. *Drugs* 73:989-997, 2013

16. Oral EA, Simba V, Ruiz E et al. Leptin-replacement therapy for lipodystrophy. *N Engl J Med* 346:570-578, 2002

17. Chatterjee S, Ganini D, Tokar EJ et al. Leptin is key to peroxynitrite-mediated oxidative stress and Kupffer cell activation in experimental non-alcoholic steatohepatitis. *J Hepatol* 58:778-784, 2013

18. Moitra J, Mason MM, Olive M et al. Life without white fat: a transgenic mouse. *Genes Dev* 12:3168-3181, 1998

19. Gavrilova O, Leon LR, Marcus-Samuels B et al. Torpor in mice is induced by both leptin-dependent and -independent mechanisms. *Proc Natl Acad Sci U S A* 96:14623-14628, 1999

20. Kim JK, Gavrilova O, Chen Y, Reitman ML, Shulman GI. Mechanism of insulin resistance in A-ZIP/F-1 fatless mice. *J Biol Chem* 275:8456-8460, 2000

21. Nunez NP, Oh WJ, Rozenberg J et al. Accelerated tumor formation in a fatless mouse with type 2 diabetes and inflammation. *Cancer Res* 66:5469-5476. 2006

22. Nunez NP, Hursting SD, Yakar S, Fowler D, Vinson C. Obesity provides a permissive

milieu in inflammation-associated carcinogenesis: analysis of insulin and IGF pathways. *Methods Mol Biol* 512:29-37, 2009

23. Yang SJ, IglayReger HB, Kadouh HC, Bodary PF. Inhibition of the chemokine (C-C motif) ligand 2/chemokine (C-C motif) receptor 2 pathway attenuates hyperglycaemia and inflammation in a mouse model of hepatic steatosis and lipoatrophy. *Diabetologia* 52:972-981, 2009

24. Yamauchi T, Kamon J, Waki H et al. Globular adiponectin protected ob/ob mice from diabetes and ApoE-deficient mice from atherosclerosis. *J Biol Chem* 278:2461-2468, 2003

25. Yamauchi T, Nio Y, Maki T et al. Targeted disruption of AdipoR1 and AdipoR2 causes abrogation of adiponectin binding and metabolic actions. *Nat Med* 13:332-339, 2007

26. Iwabu M, Yamauchi T, Okada-Iwabu M et al. Adiponectin and AdipoR1 regulate PGC-1alpha and mitochondria by Ca(2+) and AMPK/SIRT1. *Nature* 464:1313-1319, 2010

27. Yamauchi T, Tobe K, Tamemoto H et al. Insulin signalling and insulin actions in the muscles and livers of insulin-resistant, insulin receptor substrate 1-deficient mice. *Mol Cell Biol* 16:3074-3084, 1996

28. Goda N, Suzuki K, Naito M et al. Distribution of heme oxygenase isoforms in rat liver. Topographic basis for carbon monoxide-mediated microvascular relaxation. *J Clin Invest*

101:604-612, 1998

29. Takamoto I, Terauchi Y, Kubota N et al. Crucial role of insulin receptor substrate-2 in compensatory beta-cell hyperplasia in response to high fat diet-induced insulin resistance. *Diabetes Obes Metab* 10:147-156, 2008

30. Kubota N, Terauchi Y, Yamauchi T et al. Disruption of asiponectin causes insulin resistance and neointimal formation. *J Biol Chem* 277:25863-25866, 2002

31. Sartipy P, Loskutoff D. Monocyte chemoattractant protein 1 in obesity and insulin resistance. *Proc Natl Acad Sci U S A* 100:7265-7270, 2003

32. Chen A, Mumick S, Zhang C et al. Diet induction of monocyte chemoattractant protein-1 and its impact on obesity. *Obes Res* 13:1311-1320, 2005

33. Li SL, Reddy MA, Cai Q et al. Enhanced proatherogenic responses in macrophages and vascular smooth muscle cells derived from diabetic db/db mice. *Diabetes* 55:2611-2619, 2006

34. Seki E, de Minicis S, Inokuchi S et al. CCR2 promotes hepatic fibrosis in mice. *Hepatology* 50:185-197, 2009

35. Mandrekar P, Ambade A, Lim A, Szabo G, Catalano D. An essential role for monocyte chemoattractant protein-1 in alcoholic liver injury: regulation of proinflammatory cytokines

and hepatic steatosis in mice. *Hepatology* 54:2185-2197, 2011

36. Kaneko K, Ueki K, Takahashi N et al. Class IA phosphatidylinositol 3-kinase in pancreatic beta cells controls insulin secretion by multiple mechanisms. *Cell Metab* 12:619-632, 2010

37. Di Gregorio GB, Yao-Borengasser A, Rasouli N et al. Expression of CD68 and

38. macrophage chemoattractant protein-1 genes in human adipose and muscle tissues: association with cytokine expression, insulin resistance, and reduction by pioglitazone. *Diabetes* 54:2305-2313, 2005

39. Chacon MR, Fernandez-Real JM, Richart C et al. Monocyte chemoattractant protein-1 in obesity and type 2 diabetes. Insulin sensitivity study. *Obesity* 15:664-672, 2007

40. Dubois PM, Palmer D, Webb ML, Ledbetter JA, Shapiro R. Early signal transduction by the receptor to the chemokine monocyte chemotactic protein-1 in a murine T cell hybrid. *J Immunol 1*56:1356-1361, 1996

41. Bost F, Aouadi M, Caron L et al. The extracellular signal-regulated kinase isoform ERK1 is specifically required for in vitro and in vivo adipogenesis. *Diabetes* 54:402-411, 2005

42. Garg A. Acquired and inherited lipodystrophies. *N Engl J Med* 350:1220-1234, 2004

43. Nara N, Nakayama Y, Okamoto S et al. Disruption of CXC motif chemokine ligand-14 in mice ameliorates obesity-induced insulin resistance. *J Biol Chem* 282:30794-30803, 2007

44. Chemey DZ, Scholey JW, Sochett E et al. The acute effect of clamped hyperglycemia on the urinary excretion of inflammatory cytokines/chemokines in uncomplicated type 1 diabetes: a pilot stuey. *Diabetes Care* 34:177-180, 2011

45. Cai K, Qi D, Hou X et al. MCP-1 upregulates amylin expression in murine pancreatic beta-cells through ERK/JNK-AP1 and NF-kappa-B related signaling pathways independent of CCR2. *PLoS One* 11:19559-19563, 2011

46. Werle M, Schmal U, Hanna K, Kreuzer J. MCP-1 induces activation of MAP-kinases ERK, JNK and p38 MAPK in human endothelial cells. *Cardiovasc Res.* 56:284-292, 2002

47. Kang K, Reilly SM, Karabacak V et al. Adipocyte-derived Th2 cytokines and myeloid PPARdelta regulate macrophage polarization and insulin sensitivity. *Cell Metab* 7:485-495, 2008

48. Obstfeld AE, Sugaru E, Thearle M et al. C-C chemokine receptor 2 (CCR2) regulates the hepatic recruitment of myeloid cells that promote obesity-induced hepatic steatosis. *Diabetes* 59:916-925, 2010

49. Tamura Y, Sugimoto M, Murayama T et al. Inhibition of CCR2 ameliorates insulin resistance and hepatic steatosis in db/db mice. *Arterioscler Thromb Vasc Biol* 28:2195-2201, 2008